

Article

Compilation of Regional Homogeneous Seismic Catalog for Identification of Tsunamigenic Zones in the Black Sea Region

Emil Oynakov ¹, Liliya Dimitrova ¹, Lyubka Pashova ^{1,*} and Dragomir Dragomirov ^{1,2}

¹ National Institute of Geophysics, Geodesy and Geography—Bulgarian Academy of Sciences (NIGGG—BAS), 1113 Sofia, Bulgaria; emil.ilievmg@gmail.com (E.O.); lidim@geophys.bas.bg (L.D.); drago.n.dragomirov@gmail.com (D.D.)

² Department of Earth and Environmental Sciences, Ludwig Maximilian University of Munich (LMU), 80539 München, Germany

* Correspondence: lpashova.nigg@gmail.com

Abstract: Although tsunamis in the Black Sea are rare and less destructive, recently, their study has been the subject of interest due to the increasing concentration of population and infrastructure in low-lying coastal areas. This study aims to elucidate the spatial–temporal characteristics of earthquakes in the Black Sea region (27° E–42° E and 40° N–47° N) over a century to clarify the seismicity pattern further to be used for probabilistic seismic and tsunami hazard analysis. Significant volumes of seismic data from international and national databases were analyzed, and the results obtained from previous research were supplemented and expanded. Earthquakes over the period 1905–2022 from eight up-to-date seismic catalogs were used to compile a unified catalog after conversion to the moment magnitude scale M_w . The best-fit linear relationship between several magnitude scales and M_w was determined using the general orthogonal regression (GOR) and the least squares method (LSM). After the declustering procedure, the compiled catalog consists of 18,528 unique events. To assess the catalog data quality, the magnitude of completeness M_c was estimated for the entire catalog (1905–2022) and the so-called instrumental catalog (1977–2022). In addition, the spatial distribution of the completeness magnitude M_c and the recurrence b -plot slope in the Gutenberg–Richter distribution law were assessed using the goodness-of-fit and maximum likelihood methods from the instrumental catalog data. Finally, the most significant earthquakes within the Black Sea boundaries were estimated with their parameters and focal mechanisms. A possibility of the realization of strong quakes in the near future with tsunamigenic potential in the Black Sea region was concluded.

Keywords: seismicity; seismic catalog; statistical methods; tsunamigenic potential; Black Sea



Citation: Oynakov, E.; Dimitrova, L.; Pashova, L.; Dragomirov, D. Compilation of Regional Homogeneous Seismic Catalog for Identification of Tsunamigenic Zones in the Black Sea Region. *Geosciences* **2023**, *13*, 221. <https://doi.org/10.3390/geosciences13080221>

Academic Editors: Marinos Charalampakis and Jesus Martinez-Frias

Received: 22 June 2023
Revised: 15 July 2023
Accepted: 20 July 2023
Published: 25 July 2023



Copyright: © 2023 by the authors. Licensee MDPI, Basel, Switzerland. This article is an open access article distributed under the terms and conditions of the Creative Commons Attribution (CC BY) license (<https://creativecommons.org/licenses/by/4.0/>).

1. Introduction

Adequate quantification of tsunami risk on populated seashores is a theoretical and practical problem in the Earth sciences. The consequences of the tsunamis in the Indian Ocean in 2004, Tohoku, Japan, in 2011, Sulawesi, Indonesia, in 2018, and the Aegean Sea in 2020 showed that the underestimating of this hazard has led to catastrophic long-term effects for coastal populations, the economy, and the environment [1–4]. The lack of reliable historical data on tsunami occurrences, characteristic of many coasts, stimulated the development of methods for assessing the tsunami hazard and the risk based on information about the seismic activity described in the scientific literature [5–7], as well as magnitude scales for tsunamis [8]. Modern methods for calculating the maximum heights of tsunami waves with a particular frequency are based on the statistics of known tsunami events, instrumental measurements, historical data, and oral accounts of eyewitnesses.

The analysis of tsunamis in the Black Sea region has been the subject of scientific interest in the past several decades due to the increasing concentration of population, the construction of infrastructure, and tourist sites in low-lying coastal areas [9–12]. Although there have been no observations of strong or catastrophic effects of tsunami waves in the

Black Sea compared to other parts of the world, such as the Pacific and Indian Oceans, in the last century, there are historical tide gauge records of tsunami events at specific coastal locations in the study area. Such events are, for example, due to offshore earthquakes in 1927 and 1966 close to the northern and northeastern coast of the Black Sea [12]. Another tsunami phenomenon occurred after the very strong earthquake on land known as the Erzincan earthquake in 1939, when the sea receded in the coastal cities of Ordu, Fatsa, and Uniye (Northern Turkey) by about 15 m, 50 m, and 100 m, respectively, and then it advanced to the land [13].

Experimental research through numerical modeling and simulation under different scenarios is a necessary step to clarify the tsunamigenic potential in the Black Sea region due to the small number of tsunamis documented in the chronicles and the limited number of recorded post-earthquake events through continuous tide-gauge observations along the coast [14–17]. Many studies have been published in the scientific literature using different software programs for single or multiple-event numerical model simulations, different input parameters for earthquakes or other sources generating tsunamis (subaerial or submarine landslides, meteorological phenomena, etc.), various scenarios, and different spatial and temporal resolutions of the data used [18–25]. However, targeted studies of seismogenic faults as a major source that can trigger tsunamis are very rare. For example, such analyses have been conducted for specific coastal locations, such as those in [26–30]. In the case of commercial oil and natural gas exploration, e.g., [31], the data are difficult to access for scientific research.

In scientific studies, modeling and simulations of tsunamigenic phenomena in the Black Sea region are necessary to consider different tsunamigenic geometric dimensions, correctly interpret different responses at distant and local sources, and reliably determine the input parameters of the source zones. The lack of digital and analog pen-and-paper records from tide gauge stations along the coast further limits achieving a certain accuracy of the estimated wave parameters. For this reason, recent tsunami hazard and risk assessment studies of the entire Black Sea region are usually performed with a dataset of varying quality and completeness regardless of what source they are generated from and are based on previously published data or research [9,12,16,22,24,32]. More than 20 tsunami events, established from the recorded and described historical data in the scientific literature, were mainly caused by earthquakes in the coastal zone or on land near the coastline of the Black Sea. Therefore, the availability of a complete and comprehensive earthquake catalog for a specific study area is a prerequisite for performing a qualitative and thorough probabilistic seismic and tsunami hazard analysis. Furthermore, each seismic catalog is an essential source of information about the background earthquakes and earthquake sequences in the studied region and its local sub-areas, with specific seismotectonic settings [6].

Several publications on historical Black Sea seismicity and tsunami catalogs report earthquakes of a magnitude greater than 7 ($M \geq 7$) [8,22,32], most of which have generated tsunamis in the past. From 1650 to the present, evidence of five moderate intensity $4 \leq K < 7$ tsunamis on the 12-point tsunami intensity scale has been identified [8]. According to the study of Triantafyllou et al. [32] for tsunami intensities 5, 6, and 7 in the Black Sea, the return periods in this basin are 46, 128, and 1660 years, respectively.

In order to determine the seismogenic zones in the Black Sea region that can cause tsunamis, it is necessary to analyze a lot of geological, tectonic, and seismological information, which is assumed to be complete, accurate, and reliable for scientific conclusions. Therefore, a homogeneous data set of seismic events in the study area related to activated tectonic faults or their segments and properly defined earthquake parameters is needed to determine the seismogenic sources. These requirements are often difficult to meet from the available observational data. Although tectonic fault databases have been developed, such as those presented in [33,34], a comprehensive study of individual seismogenic zones in the Black Sea Basin with a detailed exploration of active faults related to their tsunamigenic potential is still limited or at an initial stage, as described above.

Following this trend, this study aims to analyze the spatial and temporal seismic activity from 1905 to 2022 in the Black Sea region and adjacent coastal territories as potential tsunami sources supplementing the research presented by Dimitrova et al. [35]. As a first step for a detailed assessment of the tsunamigenic potential of fault zones in the Black Sea region, Section 2 presents the study region, data, and methods used to compile a regional seismic catalog called the Black Sea Earthquake (BSE) catalog, which is described in Section 3. The catalog has been compiled using earthquake bulletins published by the international data centers ISC, GCMT, USGS, EMSC, Romanian and Turkish catalogs, and earthquake bulletins extracted from scientific publications. In addition, the newly compiled Bulgarian national catalog by Solakov et al. [36] has also been added to the produced earthquake catalog. The unification of the seismic events from the used catalogs was performed after converting the different magnitude scales into moment magnitude for five distinct geographical polygons. The obtained results polygon by polygon are given in Section 4. Next, the completeness and quality of a newly compiled catalog have been assessed and discussed in Section 5. In addition, we investigated the distribution of the strongest earthquakes ($M_w \geq 5$) that occurred offshore and inland in the Black Sea region. With focal mechanisms and spatial distribution of the b -values assessed from a newly compiled regional seismic catalog of completeness, an interpretation of future seismic activity is suggested. Section 6 reviews the newly compiled catalog and its applications for other seismicity and hazard assessment investigations in the Black Sea region. Finally, some inferences related to the tsunamigenic potential of earthquake sources are summarized in the conclusion section.

2. Study Region

For the presented study, we outlined a region within the boundaries 27° E – 42° E and 40° N – 47° N covering the Black Sea basin (Figure 1). Seismic sources and zones in the Black Sea region, including those with tsunamigenic potential, are defined according to various indicators presented in the scientific literature. Different zoning schemes have been proposed depending on the seismic sources of tsunamis. For example, Rangelov and Gospodinov [37] suggested that the primary seismic sources are located in the Eastern, North Caucasus, Crimea, Shabla-Kaliakra and the Southern part of the basin. Based on the maps of earthquake locations and the zones with active tectonics, Moldovan et al. [22] suggested seismic zoning consisting of ten areas with different spatial extents and seismic sources falling in and along the Black Sea coast.

In this study, we conditionally divide the Black Sea region into five sub-areas (polygons), shown in Figure 1, following the Grünthal and Wahlström approach [37]. These polygons are a Northwestern Polygon (NWP) covering the territory of eastern Romania, southern Moldova and Southwestern Ukraine; a Northern Polygon (NP) covering Southeastern Ukraine and Southern Russia; an Eastern Polygon (EP) covering Southeastern Russia and Western Georgia; a Southern Polygon (SP) covering Northern Turkey; and a Western Polygon (WP), covering the eastern coast of Bulgaria. The grounds for such zoning are based on following the coastal state borders and almost coincide with those of the exclusive economic zones of the individual countries, as Ukrainian and Russian are united, within which the local seismic catalogs are preferably prepared. In each of the polygons thus selected, data from one or more seismic catalogs were used to ensure a sufficient number of seismic events with reliably determined parameters.

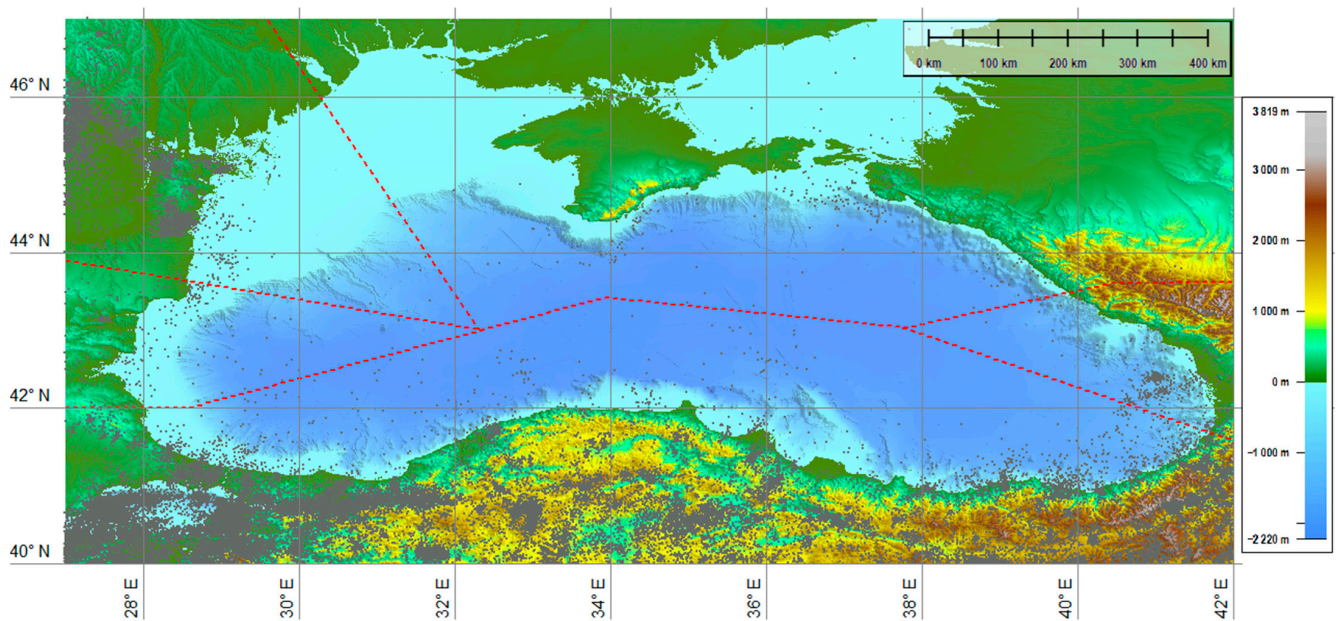


Figure 1. Location and topography of the study Black Sea region. It is divided into five polygons denoted by NWP, NP, EP, SP, and WP, the boundaries of which are indicated by a dashed red line. Earthquakes with magnitude $M \geq 1.0$ from 1905 to 2022 extracted from international and national seismic data sources are shown with tiny gray dots (more explanations are given in Section 3).

3. Materials and Methods

3.1. Seismic Datasets

Updating and maintaining magnitude-homogeneous earthquake catalogs is an ongoing commitment of international and national seismic services. The goal is to integrate local data sources on a region-by-region basis in any current catalog, selecting sources by hierarchy and applying established empirical models to convert magnitudes from disparate locally reported scales to a standard proxy magnitude scale, equivalent to a moment magnitude M_w [38]. However, inevitable changes in the configuration of national seismic networks and analysis procedures lead to bias in the hypocenter parameters of recorded earthquakes and the uncertainty estimates reported in such catalogs.

Over the past few decades, the monitoring and analysis of regional seismicity have been greatly improved by upgrading and densifying the national seismic networks of coastal countries in the Black Sea region. The earthquake catalogs covering the study area's seismic activity have been compiled and unified by various international and national institutions (as mentioned in Section 2), providing services for real-time seismic events and other seismic products. Unlike a previous study by Dimitrova et al. [35] in which seismic events with a magnitude of $M \geq 3$ were analyzed for the period AD 20–2021, this one uses collected earthquake records from more sources, including earthquakes with a magnitude of $M \geq 1$ from the beginning of the last century (1905–2022). We used data from nine up-to-date global and local earthquake catalogs, namely:

1. International Seismological Centre (ISC) catalog (<http://www.isc.ac.uk/iscbulletin/search/catalog/>) (accessed on 1 June 2023). The ISC catalog includes the earthquakes that have occurred globally since the beginning of the last century. The ISC Bulletin is updated periodically [39,40]. Some of the agencies providing data to ISC are the United States Geological Survey's National Earthquake Information Center (NEIC) and the International Data Center (IDC) of the Comprehensive Nuclear-Test-Ban Treaty Organization;
2. Global Centroid Moment Tensor (GCMT) catalog (<https://www.globalcmt.org/CMTsearch.html>) (accessed on 1 June 2023), which contains more than 25,000 earthquakes with magnitude $M > 5$ since 1976 globally [41,42];

3. United States Geological Survey (USGS) catalog (<https://earthquake.usgs.gov/earthquakes/search/>) (accessed on 1 June 2023);
4. European Mediterranean Seismological Centre (EMSC) catalog (<https://www.emsc-csem.org/Bulletin/search.php?filter=yes>) (accessed on 2 June 2023) [38];
5. Bulgarian national homogeny catalog (http://www.niggg.bas.bg/wp-content/uploads/2021/10/eq_catalogue_2022_1.pdf) (accessed on 20 May 2023) [36];
6. Turkish GSHAP catalog (2000). Turkish catalog of significant earthquakes provided for GSHAP. Available at Swiss Seismological Service, Swiss Federal Institute of Technology, Zurich, Switzerland (www.seismo.ethz.ch/gshap/turkey/seigshap.prm) (accessed on 2 June 2023);
7. Catalog of the Turkish Bogazici University KOERI, Regional Earthquake-Tsunami Monitoring Center, <http://www.koeri.boun.edu.tr/sismo/2/earthquake-catalog/> (1900–2021) (accessed on 22 May 2023);
8. Romanian catalog (Romplus) (<http://www.infp.ro/data/romplus.txt>) (accessed on 20 May 2023). The catalog is currently updated. Additionally, we used data from Oncescu et al. [43];
9. For the Northern Black Sea coast region, we used the calculated hypocentral parameters of earthquakes in the region by Kozinenko et al. [44] and Pustovitenko et al. [45–54].

Table 1 describes the local catalogs used in the polygons and their time range. The global catalogs (1), (2), (3), and (4) are used in all polygons for the cited periods.

Table 1. Seismic data catalogs used in this study.

Polygon	Time Range	Source Catalogs
Northwestern (NWP)	1900–2022	(8), (4), (9), (1), (3), (2) *
Northern (NP)	2006–2020	(9), (4), (1), (3), (2) *
Eastern (EP)	2006–2020	(9), (4), (1), (3), (2) *
Southern (SP)	1900–2021	(7), (6), (4), (1), (3), (2) *
Western (WP)	1981–2021	(5), (4), (1), (3), (2) *

* The catalogs used are sorted by priority.

The seismic events extracted from the catalogs used in this study have different parameters and magnitude scales, such as mb, MPVA, ML, Ms, md, and unreported type of magnitude or without magnitude. The data set used in this study contains 54,918 earthquakes; a significant number of them, 46,532, are without specified magnitude. The minimum magnitude values of analyzed events are equal to that in the individual catalogs. For all used catalogs, the magnitude estimates from different scales are reported in Table 2.

Table 2. Types of the magnitude scales in the catalogs.

Scale	Number of Earthquakes	Description
Mw	3436	Moment magnitude
mb	1071	Short-period body wave magnitude
MPVA	12	Regional short-period body wave magnitude
ML	1930	Richter magnitude
Ms	48	Surface wave magnitude
md	1853	Duration magnitude
M	36	Unreported type magnitude
No magnitude	46,532	

3.2. Methods

The compilation and homogenization of the BSE catalog are based on the five geographic polygons shown in Figure 1, with local data sources and selection hierarchies applied polygon-by-polygon given in Table 1. Different magnitude estimates were con-

verted to the more reliable and valuable scale, namely the moment magnitude M_w . The resulting magnitude is written as M_w -proxy—homogenized quantity.

The most common methods presented in the scientific literature to derive empirical relationships between different magnitudes and M_w are ordinary least squares (OLS), general orthogonal regression (GOR), and maximum likelihood (ML) [55–59]. Although each method has advantages and disadvantages compared to the others, in this study, magnitude conversion relationships were derived using the GOR procedure, which considers errors of both magnitude scales [55,56]. The GOR method minimizes the absolute difference of the residuals; therefore, the extreme values have less influence on the fit. Using such orthogonal regressed transformation of the discrete magnitude scales into a single instantaneous magnitude subsequently leads to a more realistic assessment of the seismic hazard.

We determined the empirical magnitude conversion relationship by performing regression analysis following the procedures and recommendations described by Castellaro et al. [57], Scordilis [58], and Gasperini et al. [59]. Different magnitude scales were converted into M_w -proxies based on empirically derived inter-magnitude relations via the MATLAB platform [60]. Calculations were conducted using seismic events available in the respective catalogs for each of the five polygons shown in Figure 1. The regression equation between two magnitude scales is as follows:

$$M_w = a M_i + b, \quad (1)$$

where M_i is, respectively, M_b , M_d , M_L , or M_s and M_w magnitude available in the used seismic catalogs determined by international agencies or regional or domestic networks for the same event. The empirical coefficients a and b are estimated separately by the least squares method for each of the five polygons. As a result of the evaluation, negligible bias was observed in the linear equations derived by the GOR. The residual for the i -th data point r_i is defined as the difference between the observed value (in the case magnitudes M_b , M_L , M_d , M_s), and the response y_i (in the case M_w) is identified as associated with the data error [61].

The next necessary step is to decluster the compiled BSE catalog to produce a homogenized catalog that can be used to analyze the seismicity in the region under study, hazard analyses, etc. The declustering algorithm by Reasenber [62] is applied to homogenize the earthquake catalog (1905–2022) based on connecting events in clusters according to adaptive space–time interaction zones and suggesting that both the space and time marginal components of an appropriate background field are Poissonian [63]. This declustering algorithm has been applied in several approaches to create homogenized catalogs, including for the Black Sea regions, for example, by Tan [64]. Seismic data sets have been processed by the ZMAP seismology software [65] using the MATLAB platform [60], which is routinely applied in seismological practice to evaluate catalog quality and the performance of seismic networks. In addition, uncertainties on M_c and b -value are determined using a bootstrap approach [66].

4. Results

4.1. Empirical Relation between Different Magnitude Scales

The equations obtained after applying the regression analysis method GOR are given in tabular form for each outlined polygon shown in Figure 1. The obtained empirical relations between moment magnitude (M_w -proxy) and any other magnitude in the catalogs (m_b , M_L , M_s , etc.), are given in the first column of the presented in the following tables of this Section 4. The second and the third columns are the standard deviations (degree of uncertainty) of the empirical parameters a and b . The other two columns fill out the number used in the relations and their magnitude range earthquakes. The value of the so-called linear correlation coefficient R -square is in the last column. The magnitude relations in the tables are presented graphically, and the data density is shown with a relative color scale ranging from 0–10. The used number of magnitude pairs N is indicated upper left in

each panel. The solid blue lines are the best linear fit of the regressions. The dashed lines represent the 95% ($\pm 2\sigma$) confidence interval.

4.1.1. Northwestern Polygon (NWP)

Magnitude relations between Mw (Mw-proxy) and mb, md, and ML are given in Table 3 and the three graphs in Figure 2. In the first column, the analyzed data sets are presented graphically, and in the second column, the obtained estimates of the parameters of the linear dependencies are shown. The relation md-Mw is derived using the most data set—576 pairs of earthquakes (Figure 2b) compared to the relation ML-Moment using 190 (Figure 2c) and mb-Mw—167 (Figure 2a), respectively. The largest magnitude range ($2.1 < mb < 6.6$) refers to the mb-Mw relation, and the most population of the data is in the magnitude interval from 2.0 to 4.6. A narrower range of $2.0 < md < 4.6$ refers to the md-Mw relation, where the most significant density above 5 ranges from 2 to 3.8. The relation ML-Mw refers to the narrowest range ($2.3 < ML < 4.5$), where the data population is concentrated in the magnitude range between 2.3 and 3.5. According to the correlation coefficients (R^2) and the degrees of uncertainty ($\pm 2\sigma$) in Table 3, the best correlation relates to the Moment and md magnitude scales.

Table 3. Relations between Mw (Mw-proxy) and mb, md and ML derived for the NWP.

Relation	$\pm 2\sigma$ (a)	$\pm 2\sigma$ (b)	Number of Data	Magnitude Range	R-Square
Mw-proxy = $0.9 \times mb + 0.3$	± 0.0862	± 0.2998	167	2.1–6.6	0.7223
Mw-proxy = $0.6667 \times md + 0.7667$	± 0.0008	± 0.0018	576	2.0–4.6	0.9995
Mw-proxy = $0.5 \times ML + 1.15$	± 0.0131	± 0.0400	190	2.2–4.2	0.9875

4.1.2. Northern Polygon (NP)

The inferred relations of Mw-proxy as a function of mb, ML, and MPVA are given in Table 4 and graphically in Figure 2.

The regression lines of minimum discrepancy are well correlated with the data distribution. For example, the relation between mb and Mw (Figure 3a) shows that the difference at low magnitude values ($mb = 2.1$) is 0.7, decreasing to 0.1 at $mb = 3.3$, and increases to 0.5 magnitude units at the largest values. The ML/Mw regression (Figure 3b) is determined from 46 pairs of earthquakes; the magnitude difference at $ML = 2.0$ is 0.7 at $ML = 3.3$, it is 0.2, and at high magnitude values, two scales almost coincide— $ML = 4.0$ and $Mw = 4$. The least amount of data (only 12 pairs) is used to find the linear regression MPVA/Mw (Figure 3c). The magnitude difference for all considered earthquakes is about 0.5, which is also noticeable from the regression equation obtained. The resulting relations show the strongest correlation (adjusted R-square = 0.9027) between the local magnitude ML and the moment magnitude Mw.

4.1.3. Eastern Polygon (EP)

Table 5 gives the relations Mw as a function of mb, md, ML, and MS. Figure 3 shows the graphs of the relations, respectively.

We found that all relations are linear, and the regression lines of minimal discrepancy correlate well with the data distribution. The slopes of the mb and ML regression lines are close to 1 (parameter a is almost equal to 1), and their intercept values with the vertical axis are negative (parameter b has negative values). Typically, the ML magnitude scales relate to the smaller earthquakes, which are below $ML < 4$. Data density varies between 5 and 10 according to the vertical color bar on the right side of the graph in Figure 4c. The relation between the body wave magnitude mb and Mw (Figure 4a) is related to the magnitude range above 3.3 ($3.3 < mb \leq 6.1$) as the most population of the earthquakes is below 5 ($M < 5$).

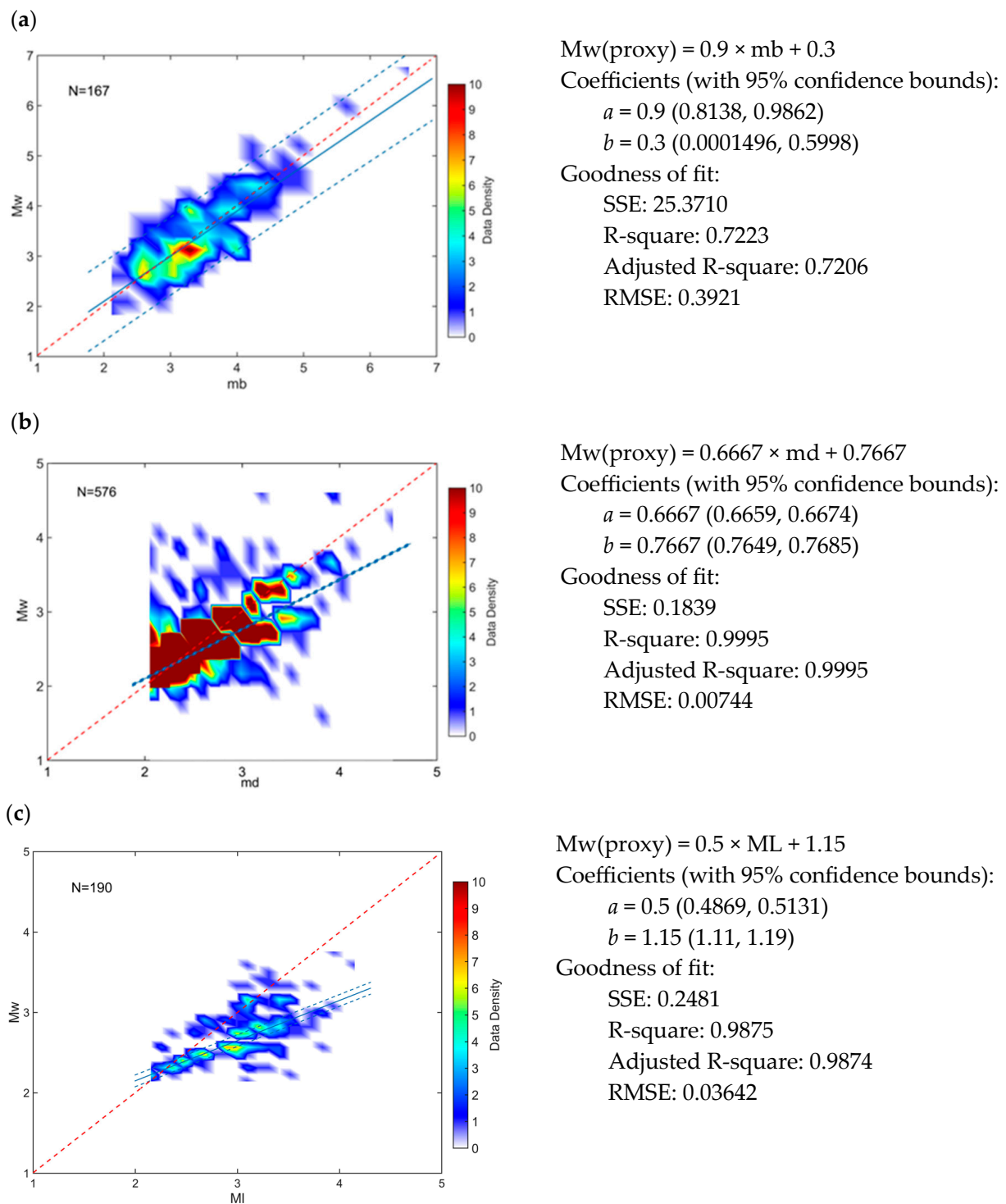


Figure 2. Magnitude relations between M_w and the other magnitude scales for the Northwestern Polygon (NWP). The **left panels** graphically represent the general orthogonal regression (GOR) with used magnitude pairs (N), and the **right** shows the linear regression estimates. Linear regression is determined for the pairs between the M_w - m_b (a), M_w - m_d (b), and M_w - M_L (c) magnitude scales, respectively. The solid blue line is the best linear fit calculated by the GOR. The dashed lines indicate the 95% confidence interval. The red line represents a 1:1 relationship between M_w and other magnitudes. Please note the scale changes along the x and y axes of the left panels.

Table 4. Relations Mw-proxy as a function of mb, ML, MPVA for the NP.

Relation	$\pm 2\sigma$ (a)	$\pm 2\sigma$ (b)	Number of Data	Magnitude Range	R-Square
Mw-proxy = $0.6117 \times mb + 1.42$	± 0.1384	± 0.4779	51	2.1–4.8	0.5829
Mw-proxy = $0.7333 \times ML + 1.133$	± 0.0764	± 0.2446	46	2.0–4.0	0.9052
Mw-proxy = $0.99 \times MPVA - 0.4995$	± 0.5741	± 2.3615	12	3.4–4.9	0.5610

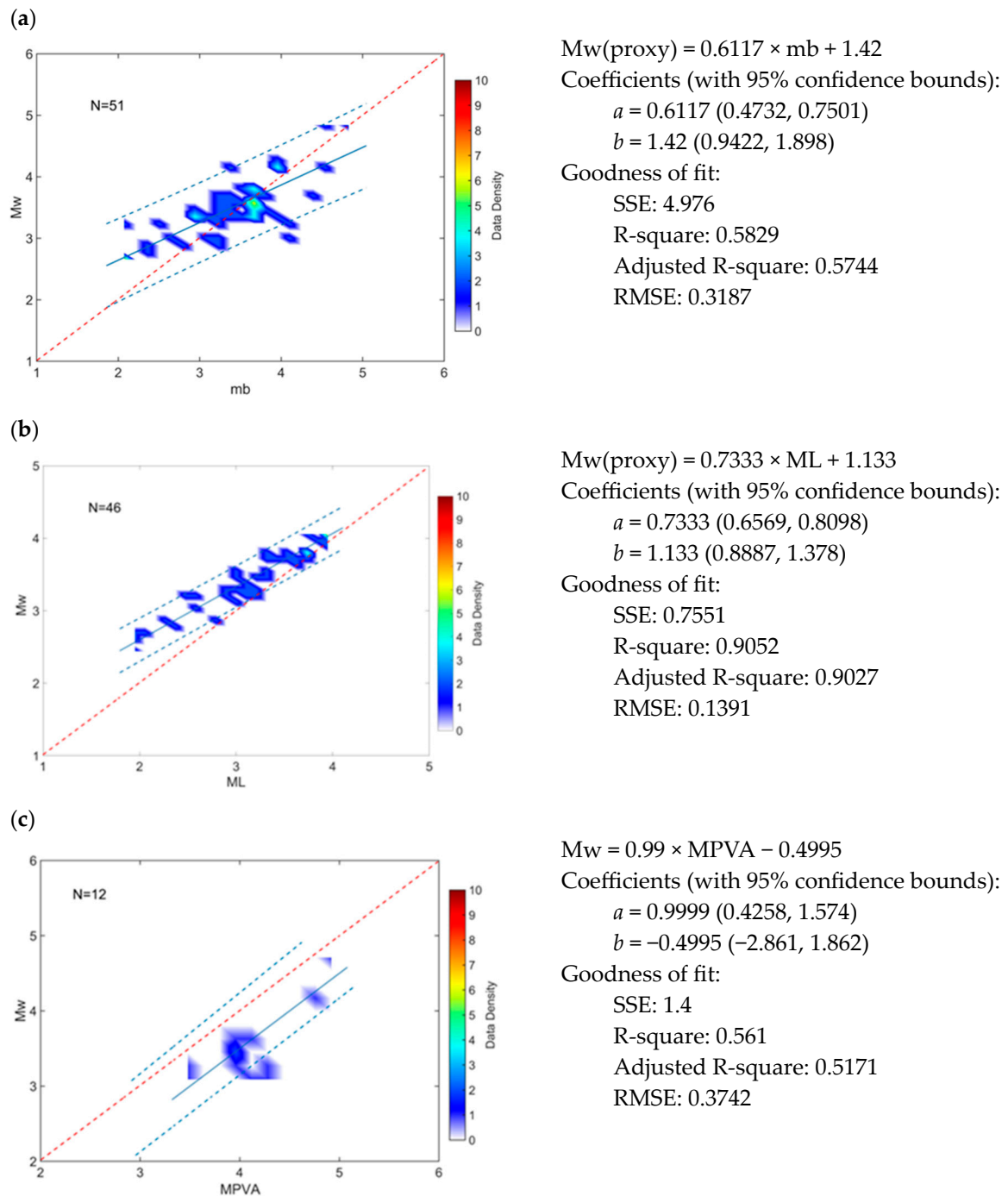
**Figure 3.** Magnitude relations between Mw and the other scales for the Northern Polygon (NP). Linear regression is determined for the pairs between the Mw-mb (a), Mw-ML (b), and Mw-MPVA (c) magnitude scales, respectively. Other notations are the same as in Figure 2.

Table 5. Relations Mw as a function of mb, md, ML, and MS for the EP.

Relation	$\pm 2\sigma$ (a)	$\pm 2\sigma$ (b)	Number of Data	Magnitude Range	R-Square
Mw-proxy = $1.064 \times mb - 0.1681$	± 0.1004	± 0.4725	41	3.3–6.1	0.9284
Mw-proxy = $1.5 \times md - 1.55$	± 0.0170	± 0.0490	463	2.0–3.4	0.9961
Mw-proxy = $1.0 \times ML - 6.064 \times 10^{-14}$	± 0.0009	± 0.0021	931	0.7–5.5	0.9997
Mw-proxy = $0.6517 \times Ms + 2.07$	± 0.0198	± 0.0875	48	2.5–6.8	0.9921

The regression line of the pair Ms/Mw has a slope of 0.7 and the b-parameter is 2.07 (Figure 4d). The relation covers the largest magnitude range from 2.5 to 6.8. It should be noted that at the smallest magnitude, the difference between Ms and Mw is greater than one magnitude unit, and at the largest magnitude, the two scales coincide.

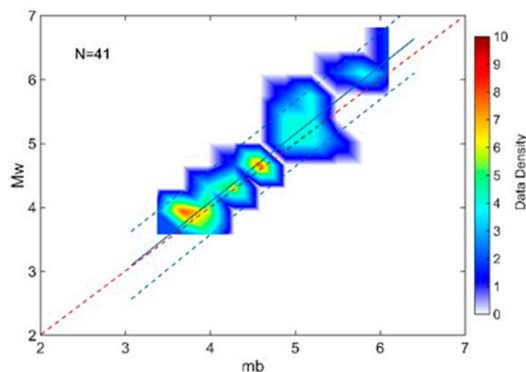
The slope of the md/Mw regression line is greater ($a = 1.5$), as shown in Figure 4b compared to the other three lines. The biggest difference is observed between the magnitudes md and Mw at the low values (0.45 magnitude units at $md = 2$); gradually, the difference decreases, and for $md = 3.1$, the two magnitude scales coincide.

For the EP, the relations Mw-mb and Mw-ML have the best correlations; the adjusted correlation coefficients R2 are close to 1, the uncertainty is minimal, and the coefficients a and b are almost equal to 1 and 0, respectively.

4.1.4. Southern Polygon (SP)

Table 6 shows the produced relations between Mw-proxy and mb, md, ML, and M based on 812, 813, 780, and 37 magnitude pairs, respectively.

(a)



$$Mw(\text{proxy}) = 1.064 \times mb - 0.1681$$

Coefficients (with 95% confidence bounds):

$$a = 1.064 (0.9632, 1.164)$$

$$b = -0.1681 (-0.6406, 0.3044)$$

Goodness of fit:

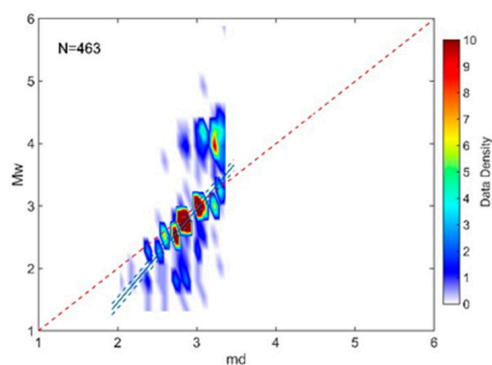
$$\text{SSE: } 2.325$$

$$\text{R-square: } 0.9284$$

$$\text{Adjusted R-square: } 0.9265$$

$$\text{RMSE: } 0.2474$$

(b)



$$Mw(\text{proxy}) = 1.5 \times md - 1.55$$

Coefficients (with 95% confidence bounds):

$$a = 1.5 (1.483, 1.517)$$

$$b = -1.55 (-1.599, -1.501)$$

Goodness of fit:

$$\text{SSE: } 0.9099$$

$$\text{R-square: } 0.9961$$

$$\text{Adjusted R-square: } 0.9961$$

$$\text{RMSE: } 0.04448$$

Figure 4. Cont.

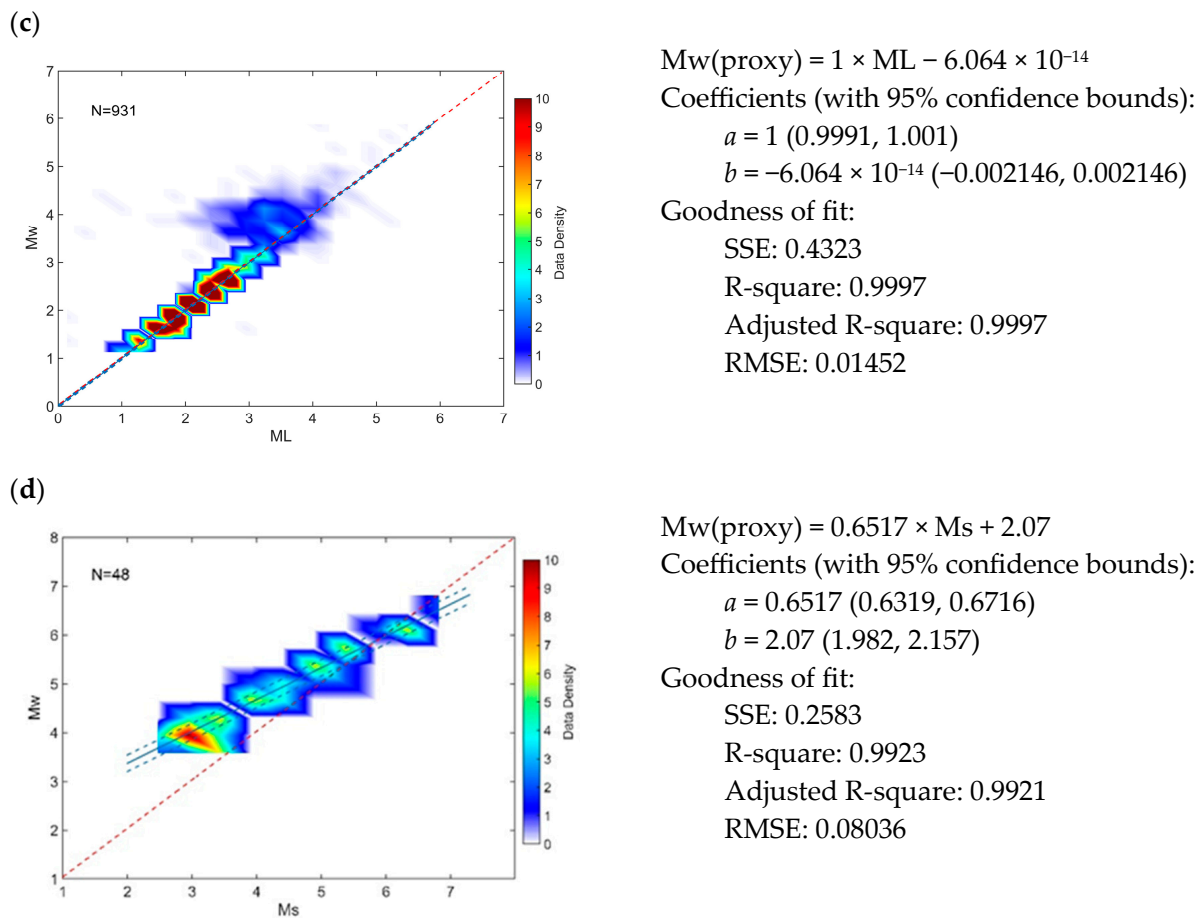


Figure 4. Magnitude relations between Mw and mb, md, ML, MS scales for the Eastern Polygon (EP). Linear regression is determined for the pairs between the Mw-mb (a), Mw-md (b), Mw-ML (c) and Mw-Ms (d) magnitude scales, respectively. Other notations are the same as in Figure 2.

Table 6. Relations between Mw-proxy mb, md, ML, and M for the SP.

Relation	$\pm 2\sigma$ (a)	$\pm 2\sigma$ (b)	Number of Data	Magnitude Range	R-Square
$Mw\text{-proxy} = 1.139 \times mb - 0.5111$	± 0.004	± 0.0149	812	2.2–5.9	0.9986
$Mw\text{-proxy} = 1.0 \times md - 0.1$	± 0.0508	± 0.0042	813	2.3–4.4	0.9992
$Mw\text{-proxy} = 1.0 \times ML + 0.00001$	± 0.0009	± 0.0019	780	2.1–4.0	0.9995
$Mw\text{-proxy} = 1.0 \times M + 0.4$	± 0.0548	± 0.2095	37	3.4–4.7	0.9776

As with the other polygons, all relations are linear, and the regression lines of minimum discrepancy are well correlated with the data distribution. The slopes of all regression lines are equal to 1 except the mb, which a-parameter is 1.139. The intercept points are minimal and equal to -0.5 and -0.1 for mb (Figure 5a) and md (Figure 5b) scales and $+0.00001$ and $+0.4$ for the ML (Figure 5c) and M (Figure 5d) magnitude scales.

The relation between ML and Mw has the best fit (Figure 5c), but it refers to the small magnitude range ($2.1 < ML < 4$). The data have the greatest density in the magnitude interval $2.1 < ML < 3.2$. The regression line almost coincides with the $y = x$ line ($b = 1.156 \times 10^{-5}$). The md/Mw regression (Figure 5b) is almost identical to the ML/Mw one. The parameters a and b are equal to 1 and -0.1 , respectively. This relation relates to magnitudes in the range $2.3 < md < 4.4$; the greatest density covers the range $2.3 < md < 3.3$.

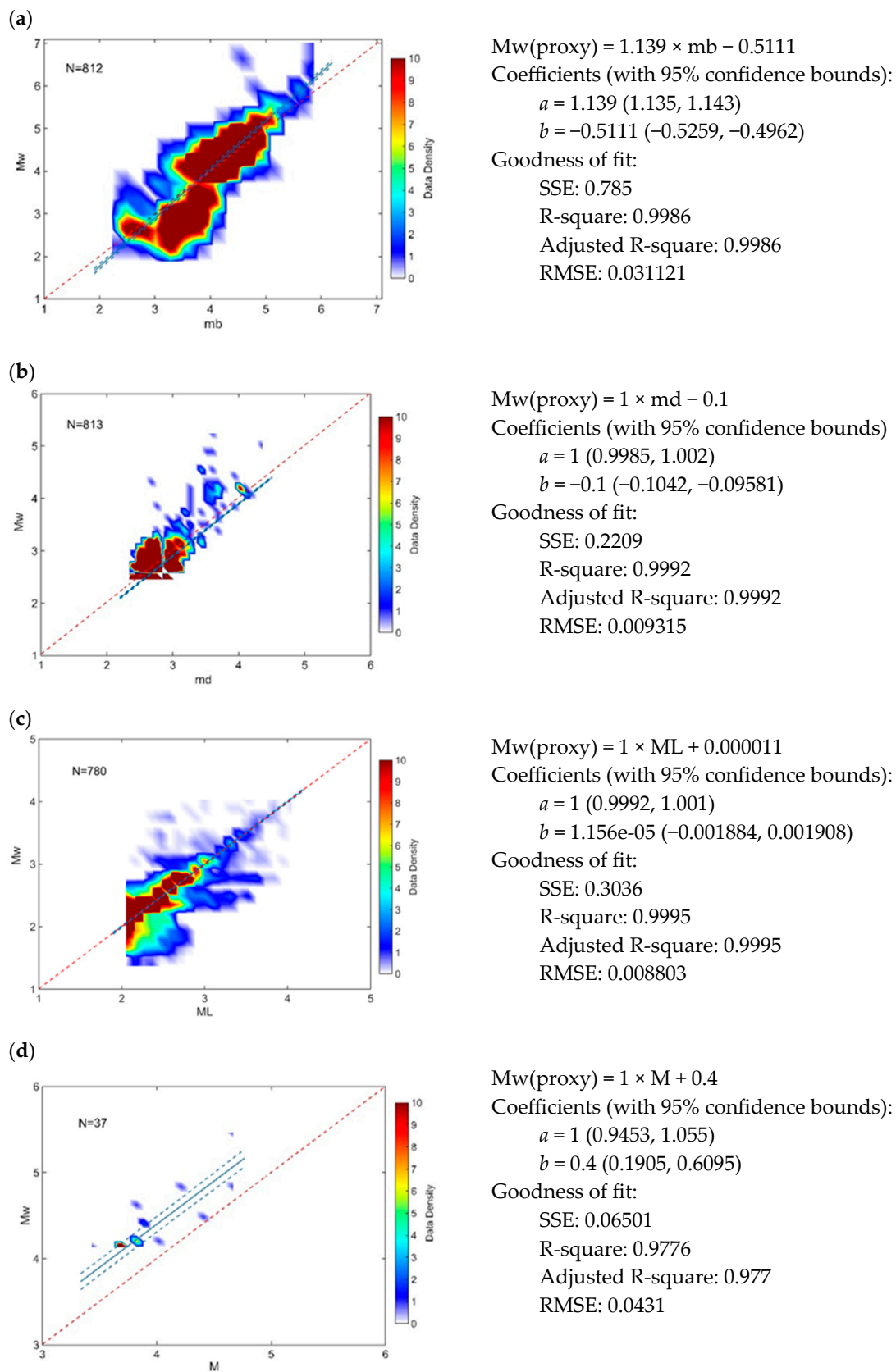


Figure 5. Magnitude relations between M_w and m_b , m_d , M_L , and M scales for the Southern Polygon (SP). Linear regression is determined for the pairs between the M_w - m_b (a), M_w - m_d (b), M_w - M_L (c) and M_w - M (d) magnitude scales, respectively. Other notations are the same as in Figure 2.

The M/M_w relation (Figure 5d) is derived based on the smallest number of data—37 pairs of earthquakes in the interval of 1.3 magnitude units— $3.4 < M < 4.7$. The magnitude scale for volume waves covers the widest range of magnitudes from $m_b = 2.2$ to $m_b = 5.8$. The relationship between m_b and M_w (Figure 5a) shows that both scales are almost the same for the lowest magnitudes; the difference is less than -0.2 and increases to 0.3 magnitude units for the largest values. The largest number of earthquakes is between 2.4 to 5.2 magnitude units.

It can be concluded that all established relations between M_w and, respectively, $m_b/md/ML/M$ have a strong correlation and could be applied to homogenize the Southern Polygon catalog data.

4.1.5. Western Polygon (WP)

The data used in this study for the Western Polygon (WP) are derived from the Bulgarian national homogenized catalog [35], as shown in Table 1. The number of earthquakes is 1023 covering the period from 1981 to 2019 in the magnitude range $M_w \geq 3.2$. The earthquakes in the Bulgarian catalog are presented in [67] by M_w magnitude scale, and we have directly included them in the compiled catalog for the Black Sea region.

5. Homogenization and Evaluation of the Completeness of the Compiled BSE Catalog

We compiled a new regional declustered catalog, including the earthquakes in the Black Sea region since the beginning of the past century. The complete catalog comprises the earthquakes with moment magnitudes M_w , if available in the downloaded catalogs used, and M_w -proxy magnitudes produced with the obtained relations, which express the best data fit. According to the maximum earth crust in the region [68], the depth of the listed earthquakes is limited to 40 km. As a result, the catalog of 54,647 events was obtained for the region $27^\circ \text{ E}–42^\circ \text{ E}$; $40^\circ \text{ N}–47^\circ \text{ N}$ covering the period 1905 to 2022. The data of these earthquakes are saved in the CSV format and proved via Zenodo on the following link: <https://zenodo.org/badge/DOI/10.5281/zenodo.8070409.svg> (accessed on 22 June 2023). The catalog has been released under an open license and integrates data from global and local earthquake catalogs based on each of the five polygons. Figure 6 shows the cumulative curve of the catalog events from 1905 to 2022. It is seen that the number of registered earthquakes exponentially increased after 1970.

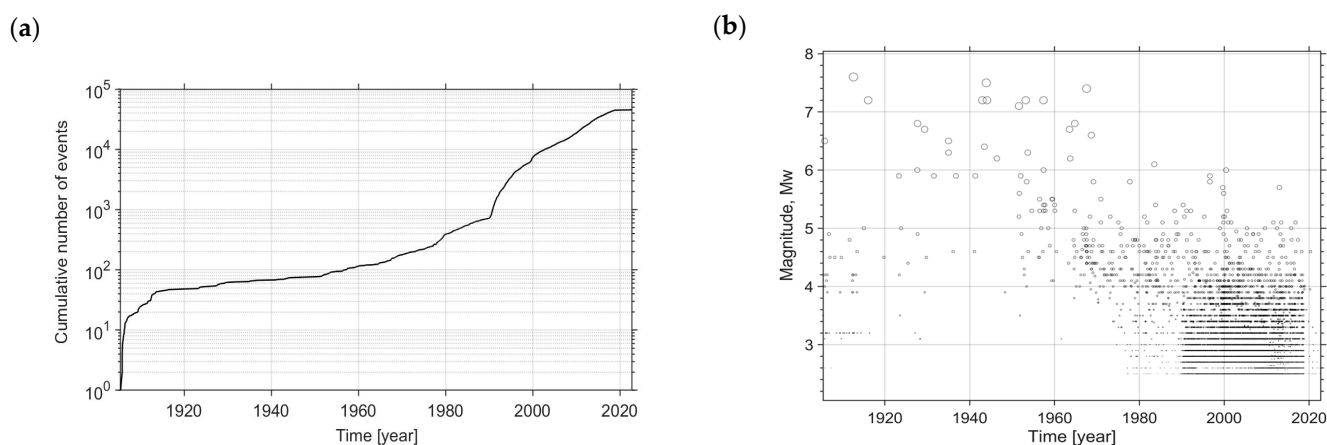


Figure 6. (a) Cumulative curve of the earthquakes collected from the used catalog, covering the 1905–2022 period; (b) magnitude distribution over time for the declustered catalog 1905–2022.

The BSE catalog contains the following information:

- Date: year, month, day;
- Origin time in standardized GMT: hour, minute, and second;
- Epicenter coordinates: Latitude $\varphi^\circ \text{ N}$ and Longitude $\lambda^\circ \text{ E}$;
- Focal depth in km;

- Moment magnitude, M_w .

To assess the catalog data quality, we estimate the magnitude of completeness M_c , which, theoretically, is the lowest magnitude above which 100% of the earthquakes in the given region and time range are detected [69]. The minimum magnitude of completeness M_c for a given catalog is an essential parameter for many studies of the seismic regime and the earthquake hazard assessment in a particular region (see, e.g., [70,71]). Before calculating the completeness magnitude [66,72], the catalog must be declustered. Applying Reasenbergs' declustering algorithm [62], the earthquakes are grouped into clusters according to spatial and temporal interaction zones in the Black Sea region, and the aftershocks and foreshocks are identified and removed. Thus, the catalog includes 18,528 unique events with $M_w \geq 1.0$. Using a non-instrumental catalog or a catalog created by merging non-instrumental and instrumental often results in a higher value of M_c due to under-sampling [65,72]. The estimated magnitude of completeness M_c is equal to 5 ($M_c = 5$). Therefore, the estimated value of M_c shows that there are earthquakes below 5, omitted in the catalog 1905–2022.

The M_c value obtained can be explained by incompleteness in the used catalogs in this study or incorrect magnitude estimations, especially around the 70s of the last century. This assumption is supported by the distribution of magnitude estimates over time for the declustered 1905–2022 catalog depicted in Figure 6b. This Figure shows that till the middle of the last century, in the studied region, stronger and moderate earthquakes ($M_w \geq 4$) have been predominantly registered. Over time, the recorded magnitude gradually and steadily decreases to 2.5. The number of events in the magnitude intervals is as follows: 49,040 are in $3 > M_w$; 3876 are in $3.0 \leq M_w < 3.5$; 949 are in $3.5 \leq M_w < 4$, 468 are in $4.0 \leq M_w < 4.5$; 190 are in $4.5 \leq M_w < 5.0$, 72 are in $5.0 \leq M_w < 5.5$, 24 are in $5.5 \leq M_w < 6.0$, and 28 earthquakes with magnitude greater than 6 ($M_w \geq 6$).

After the first half of the past century, significant progress has been made in increasing the number of seismic stations and earthquake detection capabilities in the Black Sea region, as seen in Figure 6a. The sensitivity of national networks for recording weak earthquakes through installing modern broadband seismic stations has increased significantly, as well as the refinement of procedures and software for locating and estimating the magnitude of small to moderate earthquakes. Thus, the earthquake detection capabilities of the networks have been significantly improved. As a result, the number of recorded events has considerably increased, especially after 1980 (Figure 6a,b), and the minimum magnitudes in the catalogs have been significantly reduced. The years around 1980 can be considered as a dividing line for non-instrumental and instrumental seismic observation. As a rule, the M_c is calculated for the instrumental earthquake catalog, which is more comprehensive than the non-instrumental catalog, predominantly based on the macroseismic observations.

Based on these circumstances and after several approaches made to calculate the magnitude of completeness for different starting times, we considered that 1977 could be accepted as the starting year from which the seismic data catalogs could be used for in-depth analysis, comparison and use for seismic hazard and tsunami hazard assessment. The declustered catalog 1977–2022 comprises 18,295 earthquakes within the magnitude range from 2.5 to 6.1 ($2.5 \leq M \leq 6.1$) and a maximum depth of 40 km ($h \leq 40$ km).

Figure 7a shows the distribution of the number of earthquakes over the years in 1/12-year-long bins. The maximum number of earthquakes was in 1999, when two earthquakes of magnitude greater than 7 ($M_w > 7$) and many events of smaller magnitude occurred in SP. Figure 7b shows the magnitude distribution over time for the declustered catalog 1977–2022. It is shown that there are no missing estimates over the entire magnitude range from 2.5 to 6.1.

The number of earthquakes distributed in bins with size 0.1 is shown in Figure 7b. Most of the events in the studied region are in a magnitude range of 2.5–4.5, accounting for about 95% of the total number of events in the catalog. The largest part comprises the earthquakes with a magnitude of around 2.5 ($2.6 \geq M \geq 2.5$), and the number of the stronger earthquakes exponentially reduces.

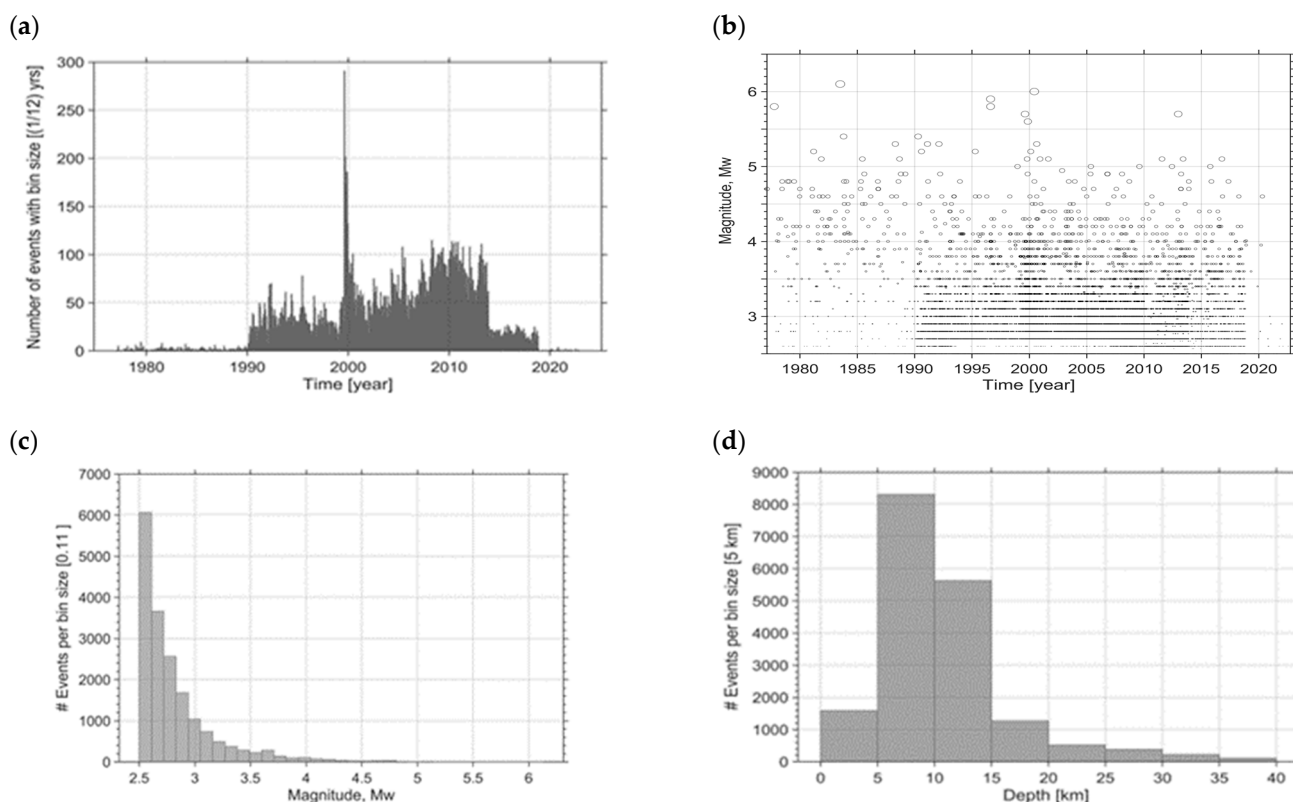


Figure 7. (a) Histogram of the number of earthquakes covering the 1977–2022 period listed in the catalog calculated in bin size of 1/12 year; (b) distribution of hypocenters in depth over time; (c) histogram of the magnitude distribution within 0.11 bin size of the magnitude; (d) histogram of depth distribution within 5 km size bins.

This trend is evidenced by the distribution of earthquakes' depths (Figure 7d), especially for depths over 5 km. The hypocenters of events in the compiled catalog are distributed, respectively: 4133 events (7.6%) within the range 1–5 km, 30,041 (55%) are from 5 km to 10 km, 17,446 events (32%) are from 10 km to 20 km, and 3027 (5.5%) are below 20 km, as shown in Figure 7d. Moreover, 85% (105) of earthquakes with $M_w \geq 5$ were identified in the 10–40 km depth range.

The magnitude of completeness M_c is estimated using the maximum curvature method with bootstrapping [65,66]. The frequency–magnitude distribution (FMD) of the earthquakes listed in the declustered catalog from 1977 to 2022 is modeled using the Gutenberg–Richter power law shown in Figure 8a. The FMD of the data fits the synthetic distribution well, plotted as a red line. The more considerable differences are in magnitudes above 5.1 ($M_w > 5.1$), where a simple power law cannot adequately explain the observed FMD. The calculated parameters of the values of b and a are 1.17 ± 0.01 and 7.192, respectively. Therefore, considering the completeness of M_c , b -value, and a -value, we can conclude that all earthquakes with a magnitude above 2.5 ($M_w \geq 2.5$) are reliably recorded and presented in the newly compiled catalog.

The right panel of Figure 8b presents the variations of the magnitude completeness M_c over the years. The temporal variation of M_c is estimated using a window with 500 events and a step of 25 events. The standard deviation of the M_c is depicted with a black dashed line, and it is not more than 0.2 ($M_c \pm \sigma$: $M_c \pm 0.1$). Considering Figure 8b, the completeness magnitude is very stable over the years.

Figure 9a shows the spatial distribution of the completeness magnitude within the studied region. The spatial distribution of M_c is performed on a 20 km grid and at least 100 events greater than the magnitude ($M_w > 2.5$) within a 100 km radius for each grid node. To avoid the statistical errors arising from under-sampling and inhomogeneous

data, we calculated the spatial-temporal distribution of the M_c and b -value according to Amorese et al. [73]. The completeness magnitude varies from 2.5 to 4.2.

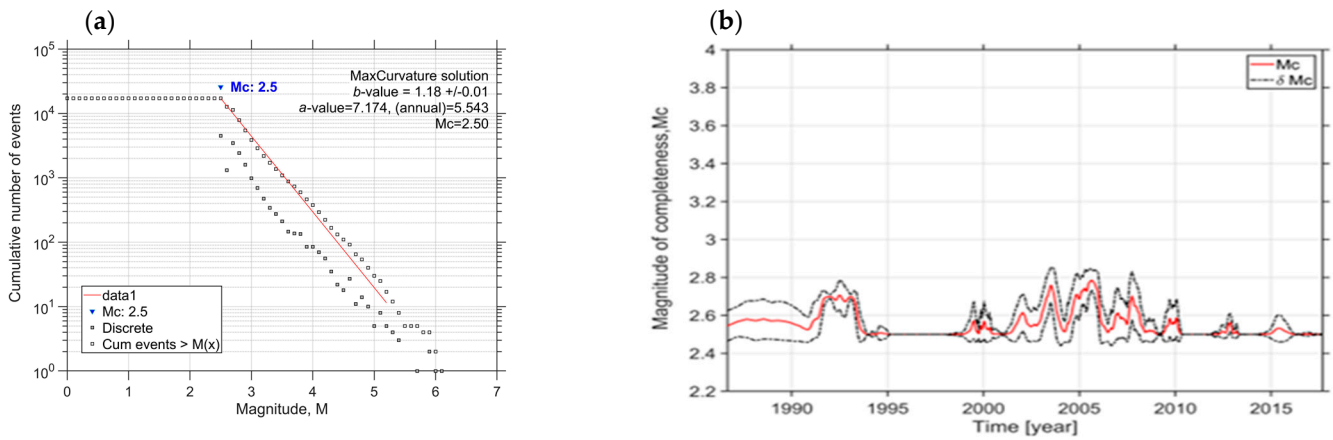


Figure 8. (a) Frequency–magnitude distribution (FMD) of the seismic events within the Black Sea region from the compiled catalog 1977–2022; (b) variations of the magnitude of completeness M_c over the years.

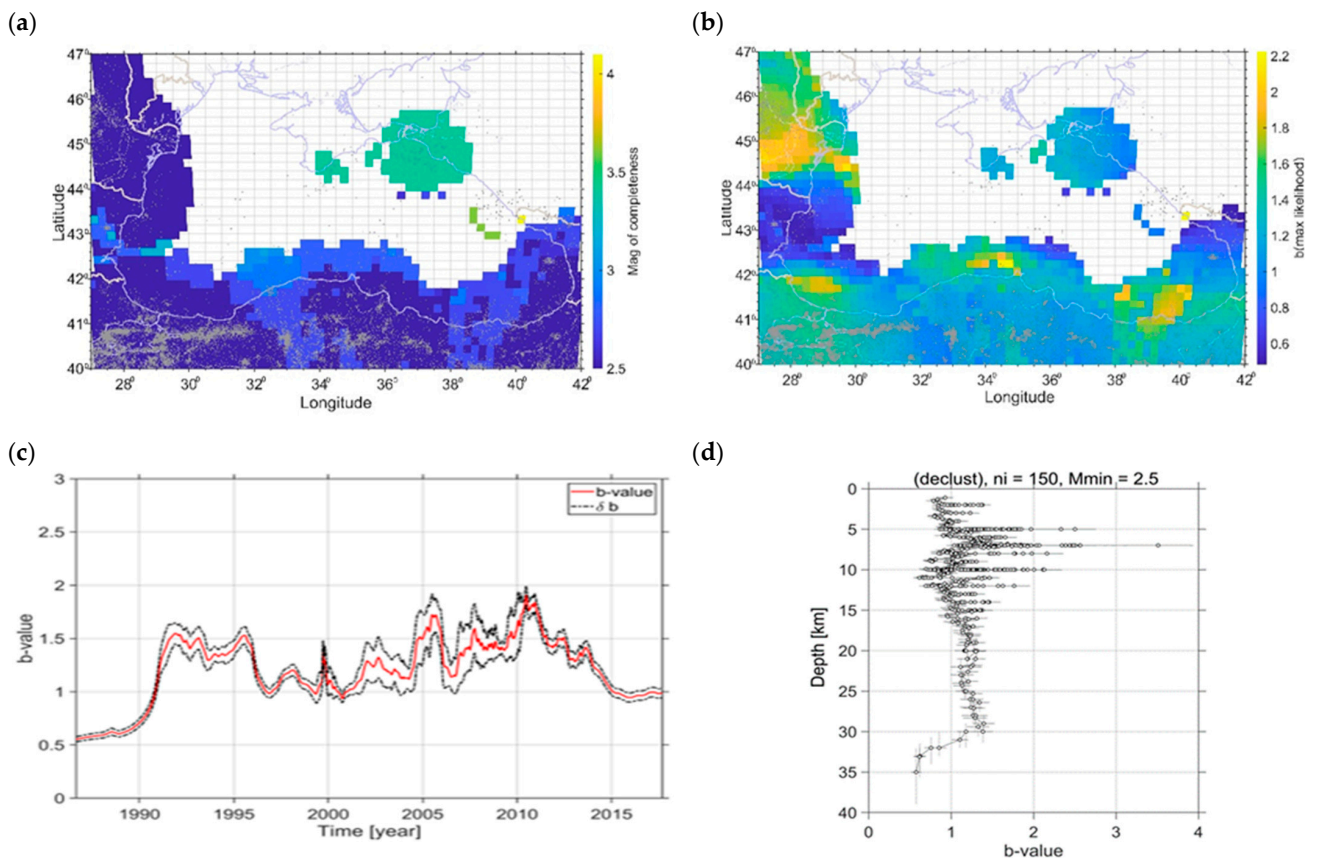


Figure 9. (a) Spatial distribution of the magnitude of completeness of the homogenized catalog 1977–2022; (b) spatial distribution of b -value distribution obtained in this stud; (c) variations of b -value over the years; (d) depth distribution of b -value.

The compiled catalog is complete for the NW, W, S, and E polygons, and the magnitude of completeness is within the interval 2.5–3.0. The higher value of M_c is likely due to the poor coverage of the local seismic networks and the not registered earthquakes with smaller magnitudes.

The value of M_c in the NP increases above 3 ($M_c > 3$) as in a few parts reaches 4.0 where there is not enough data in the catalog to fulfill the criterion for calculating the M_c . The white zones in the polygon are due to a lower level of seismicity.

Figure 9b shows the spatial distribution of the b -value, which variations are calculated using the maximum likelihood method of Aki [74]. The map is drawn with the same parameters as the map of the magnitude of completeness, i.e., executed on a 20 km grid size and at least 100 events within a 100 km radius for each grid node. Such parameters are sufficient to avoid erroneous b -value statistical results due to undersampling and inhomogeneous subsets [75–85]. As a result, relatively low b -values are obtained for the WP and the EP (see Figure 1 for the outlined polygons), while relatively high b -values characterize the SP and NWP.

The temporal variation of the b -value is shown in Figure 9c. The standard deviation is drawn with black dashed curves, and it is within ± 0.1 ($\sigma_b = \pm 0.1$). The shape of this curve largely repeats the curve of the completeness magnitude distribution over the years (Figure 8b). In both curves, the variations of the calculated b -value and M_c magnitude are strongly dependent on the maximum and minimum magnitude of realized earthquakes as well as the number of recorded earthquakes of the corresponding magnitude (Figure 7a,b).

The depth distribution of the b -value is given in Figure 9b. Variations in depth are calculated over 5 km depth layers that contain at least 150 events. The maximum b -value is at a depth of 7 km, where most of the events in the catalog are realized. There are four other peaks in the curve at depths of 5 km, 8 km, 10 km, and 12 km, and two distinct minima at 11 km and below 30 km depth. Figures 9b and 7d prove that the prevailing part of the earthquakes occurs at the depth range from 5 km to 15 km, and there are no seismically inactive layers of the Earth's crust in the study region.

6. Discussion

The Black Sea is located within the Anatolian sector of the Alpine Himalayan orogenic system. The geodynamic processes in this region are related to the northward movement of the African and Arabian plates, which collide with the Eurasian tectonic plate. The Anatolian block is moving westward with a rotational motion focused northward from the Sinai Peninsula [86]. These processes delineate specific zones of concentration of seismic epicenters along tectonic units [35,87,88]. As previously described by Oynakov et al. [89], the seismic events in the Black Sea region could be clustered into the strongest earthquakes and outlined the main seismic zones: Shabla-Kaliakra, the Crimean Peninsula, three clusters located on the eastern shores of the Black Sea (west coasts of Georgia and Russia), and one on the southern coast near Bartın, Northern Turkey. A large number of earthquakes are related to the Vrancea seismic zone. The present study demonstrates the same seismic pattern in the Black Sea region. Figure 1 shows the distribution of the denoted by grey dot epicenters. According to the compiled catalog, the hypocentral depth of the earthquakes in the study region is not more than 40 km. The strongest earthquakes above 5 ($M_w \geq 5$) are mainly realized along the Northern Black Sea coast of Turkey (offshore and on land), the Western Black Sea coast of Georgia (offshore and on land), the offshore of the Northern Bulgaria Black Sea coast and the Vrancea seismic zone.

In order to give a quality estimation of the compiled in the study catalog, we compare its parameters M_c , b -value, and a -value to such ones calculated by Dimitrova et al. [35]. The produced magnitude of completeness M_c is equal to 2.5. The value is smaller than those in [35] (hereafter, the parameters related to the catalog by Dimitrova et al. [35] will be marked with a suffix 21), namely $M_{c21} = 3.0$. The relatively lower M_c value is the result of the addition of the national catalogs of the Black Sea countries in the current catalog. As a rule, the local networks can detect and process the smaller magnitude ($M \leq 3$) events included in the local catalogs. Thus, the M_c of the newly compiled catalog was reduced to 2.5. Nevertheless, the FMD of both compiled catalogs is linear with parameters as follows: b_{21} -value = 1.09 and b -value = 1.17 (Figure 8a); a_{21} -value = 7.279 and a = 7.192 (Figure 8a). The spatial distribution of the completeness magnitude for both catalogs follows the model

of higher values in the Northeastern Black Sea region and smaller values in the west and south parts. In addition, the present study gives the spatial distribution of the M_c in more detail (Figure 9a) due to the above-explained reasons.

The spatial distribution of the b -values, calculated for both catalogs, has a similar behavior; the highest values are mapped in the eastern part of the Southern Black Sea coast. For the current catalog, there are higher b -values in the southwestern and northwestern parts of the region and distinctly low values in the eastern and western parts (Figure 9b). This behavior could be explained with more comprehensive local catalogs (Turkish, Romanian, Bulgarian).

There are several studies on the temporal and spatial variations of b -values; they reflect stress conditions [81–84] or in strong connections with the different types of faulting [84] and are considered as a precursor of upcoming small or strong events [84,85]. It was found that a high b -value indicates a higher proportion of events with smaller magnitudes and vice versa—a small b -value indicates earthquakes with larger magnitudes. In general, our results conform with those obtained by other authors cited above.

The variations of the temporal and depth distribution curves of the b -value (see Figure 9a,b) are the same as those of the corresponding curves for the b_{21} -value. The curve in Figure 9a gives a more detailed temporal distribution of the b -value, and the curve in Figure 9b is smoother than that of the b_{21} -value. The appearance of the two curves is due to the more comprehensive national catalogs included.

The most significant earthquakes in the Black Sea region, which could affect the population, infrastructure, and tourist sites in low-lying coastal areas, have a magnitude above 5 ($M_w \geq 5$). According to the compiled catalog from 1977 to 2022, these earthquakes and their parameters extracted from relevant sources are listed in Table 7. The focal mechanisms of the listed earthquakes are given in column 11, and the source is given in column 12 of the table. Unfortunately, the information on the focal moment tensor mechanisms of several earthquakes before 2000 is missing or not freely available.

Most of the earthquakes listed in Table 7 have occurred in Northern Turkey and are associated with the branches of the North Anatolian Fault Zone [86–88]. Four earthquakes (with numbers 1, 5, 8, and 25) are realized offshore in the aquatorium of the Black Sea, respectively: 1 is close to the NW coast of Turkey; 5 and 25 are close to the west coast of Georgia; 8 are close to the NE coast of Bulgaria (near Balchik). Two earthquakes (3 and 30) are related to the Vrancea seismic zone. The strongest event has a magnitude of $M_w = 6.1$ and is realized in the aquatorium of the Marmara Sea [85].

The fault plane solutions of earthquakes in the Black Sea (near the coasts of NE Bulgaria and West Georgia) have strike-slip faulting. The reverse faulting component dominates for the Southwestern Black Sea (event 1) and Western Georgia (event 4). The focal mechanism of the events realized on the mainland of Northern Turkey (eastern, central, and western parts) has a predominantly strike-slip component. Therefore, we can conclude that the focal mechanisms of the earthquakes with $M_w \geq 5.0$ in the Black Sea region agree with the primary fault neotectonics.

Several studies of the b -value show that its variations are in strong connections with the different types of faulting [81–85]. It is concluded that the areas where faults are located and subjected to greater stress (thrust faults) demonstrate a lower b -value; those with seismic events associated with normal faults and strike-slip faults have the highest and intermediate b -values, respectively. We do not notice such behavior of the b -value in the presented study. To accurately determine spatial and temporal variations in the b -value, high-precision seismic catalogs of all determined polygons are required, which is the goal of the next study.

The disruptive seismic events triggered tsunamis in the past fall within the main seismic zones outlined in the Black Sea region. According to the BSE catalog, from 1977 to 2022, a strong earthquake occurred in the offshore region of NW Turkey in the Marmara Sea in 1983 and had a magnitude $M_w = 6.1$ (see Table 7, first column, event 4).

Table 7. The earthquakes with a magnitude above 5 ($M_w \geq 5$) in the region of the Black Sea.

N	Year	Month	Day	Hour	Minute	Lat (N°)	Long (E°)	Depth (km)	Mw	Focal Tensor Mechanism	Source	Region
1	2	3	4	5	6	7	8	9	10	11	12	13
1	1977	10	5	5	34	41.126	33.6147	7.7	5.8		(1)	North Turkey
2	1981	3	12	4	6	40.8329	28.157	9	5.2	N/A		NW Turkey
3	1981	11	13	9	7	45.17	29	15	5.1		(5)	Vrancea Region
4	1983	7	5	12	1	40.3767	27.2869	10.4	6.1		(1)	Offshore NW Turkey Marmara Sea
5	1983	10	21	20	34	40.1549	29.3437	14.9	5.4		(1)	NW Turkey
6	1985	6	10	11	41	40.6797	36.0648	12.8	5.1	N/A		North Turkey
7	1988	4	24	20	49	40.9134	28.2793	13.9	5.3		(1)	NW Turkey
8	1988	9	6	19	16	42.0274	41.6671	12.3	5.1	N/A		Offshore Georgia Black Sea
9	1990	4	20	23	30	40.0219	40.0561	15.6	5.4		(1)	NE Turkey
10	1990	8	5	18	31	40.2891	33.9139	27.7	5.2	N/A		North Turkey
11	1991	2	12	9	55	40.8757	28.8232	12.4	5.3		(4)	West Turkey
12	1992	2	12	15	59	40.6179	35.8926	9.8	5.3	N/A		NW Turkey
13	1995	4	13	4	8	40.829	27.8033	25.7	5.2	N/A		NW Turkey
14	1996	8	14	1	55	40.7182	35.2232	16.5	5.8		(1)	NW Turkey
15	1996	8	14	2	59	40.7308	35.2449	15.6	5.6		(1)	NW Turkey
16	1996	8	14	3	1	40.3354	35.184	11	5.9		(1)	NW Turkey
17	1997	2	28	0	3	40.7481	35.3774	8.8	5.2		(4)	NW Turkey
18	1998	12	19	16	15	40.1216	41.9951	9	5	N/A		NE Turkey
19	1999	8	17	0	1	40.7968	29.9952	16.3	7.5		(1)	NW Turkey
20	1999	8	17	0	15	40.7018	30.8455	11	5.1		N/A	NW Turkey
21	1999	8	17	0	16	40.7308	29.9134	12	5		N/A	NW Turkey
22	1999	8	17	1	33	40.7545	29.049	11	5.6		N/A	NW Turkey

Table 7. Cont.

N	Year	Month	Day	Hour	Minute	Lat (N°)	Long (E°)	Depth (km)	Mw	Focal Tensor Mechanism	Source	Region
23	1999	8	17	2	34	40.6463	30.5892	11	5.7	N/A		NW Turkey
24	1999	8	17	2	42	40.6822	30.6152	7.8	5.4	N/A		NW Turkey
25	1999	8	17	2	50	40.796	29.9651	15.4	5.3	N/A		NW Turkey
26	1999	8	17	3	14	40.7237	30.5507	19.4	5.3	N/A		NW Turkey
27	1999	8	17	4	20	40.7101	30.348	11	5	N/A		NW Turkey
28	1999	8	17	6	28	40.8137	31.0329	11	5	N/A		NW Turkey
29	1999	8	19	15	17	40.633	29.1074	17.6	5.1		(1,2,3)	NW Turkey
30	1999	8	20	10	0	40.6578	30.5559	11	5	N/A		NW Turkey
31	1999	8	22	14	31	40.707	30.6945	11	5.3	N/A		NW Turkey
32	1999	8	31	8	10	40.7866	29.9091	6.7	5.1		(1)	NW Turkey
33	1999	9	13	11	55	40.7873	30.0853	15.7	5.9		(1)	NW Turkey
34	1999	9	20	21	28	40.7102	27.594	13.4	5.2	N/A		NW Turkey
35	1999	9	29	0	13	40.799	29.3771	14.6	5.2		(1)	NW Turkey
36	1999	10	20	23	8	40.7994	28.9655	13	5.1	N/A		NW Turkey
37	1999	11	11	14	41	40.8069	30.2183	13.1	5.7		(1)	NW Turkey
38	1999	11	12	16	57	40.8243	31.2073	14.9	7.1		(1)	NW Turkey
39	1999	11	12	17	17	40.7921	30.9896	11	5.6	N/A		NW Turkey
40	1999	11	12	17	29	40.8204	31.4463	9	5.1	N/A		NW Turkey
41	1999	11	13	0	54	40.8416	30.9473	11	5	N/A		NW Turkey
42	1999	11	16	17	51	40.7655	31.5042	12.7	5	N/A		NW Turkey
43	1999	11	17	0	15	40.8428	31.3081	11	5	N/A		NW Turkey
44	1999	11	17	8	15	40.8515	31.4997	9	5	N/A		NW Turkey
45	1999	11	20	8	44	40.8323	31.4786	9	5	N/A		NW Turkey
46	2000	2	14	6	56	41.036	31.738	10	5.2		(3)	NW Turkey
47	2000	6	6	2	41	40.7	32.982	10	6		(1)	North Turkey
48	2000	6	9	3	14	40.723	32.921	3.9	5	N/A		North Turkey
49	2000	8	23	13	41	40.782	30.76	10.5	5.3		(1)	NW Turkey
50	2000	12	7	12	16	41.409	29.362	10	5.1	N/A		Offshore NW Turkey

Table 7. Cont.

N	Year	Month	Day	Hour	Minute	Lat (N°)	Long (E°)	Depth (km)	Mw	Focal Tensor Mechanism	Source	Region
51	2001	8	26	0	41	40.958	31.544	8.8	5.1		(3)	NW Turkey
52	2005	5	12	9	25	40.4376	37.3984	5	5		(1)	NE Turkey
53	2009	8	5	7	49	43.4216	28.6636	14.5	5		(1.2)	Offshore Bulgaria Black Sea
54	2011	7	25	17	57	40.8244	27.7474	12.2	5.1		(1)	NW Turkey
55	2012	6	7	20	54	40.8459	27.9342	7.7	5		(1)	NW Turkey
56	2012	12	23	13	31	42.4407	41.0577	12.9	5.7		(1)	Offshore Georgia Black Sea
57	2012	12	25	22	44	42.4554	40.982	13.5	5.3		(1.2)	Offshore Georgia Black Sea
58	2013	5	28	0	9	43.2283	41.6351	9.2	5.1		(1)	West Georgia
59	2015	10	9	14	39	40.7005	36.687	14.3	5		(1)	North Turkey
60	2016	10	15	8	18	42.1905	30.6868	6.4	5.1		(1)	Offshore NW Turkey Black Sea

N/A means not applicable; (1) Global CMT Catalog. <https://www.globalcmt.org/> (accessed on 3 June 2023); (2) Kalafat (2018) [84]. https://doi.org/10.1007/978-3-319-77359-9_25 (accessed on 3 June 2023); (3) European-Mediterranean Regional Centroid-Moment Tensors. <http://rcmt2.bo.ingv.it/> (accessed on 3 June 2023); (4) Kalafat et al. (2009) [85]. Report (In Turkish); (5) Gobarenko et al. (2016) [25]. <https://doi.org/10.1134/S0016852116040026> (accessed on 3 June 2023).

In 1999, the strongest earthquakes with magnitudes $M_w = 7.5$ and $M_w = 7.1$ were realized on the land of NW Turkey (events 19 and 38 in Table 7). In 2000, an earthquake with magnitude $M_w = 6$ (event 47 in Table 7) was realized in N Turkey. However, there was no evidence for the realization of the tsunami waves.

Based on the spatial distribution of the b -value in the Black Sea region, which is mapped in Figure 8b, the earthquake catalog, and the information on the geodynamic potential of the faults in the Black Sea region, we could conclude that stronger earthquakes can occur in the region in the near future. Nevertheless, the tsunami frequency in the Black Sea is rated as low [9,32], and the estimated tsunami hazard in the Black Sea is low to moderate; it cannot be neglected.

The recent Triantafyllou et al. [32] study, regardless of the tsunami generation mechanisms, shows that more realistic results for a probabilistic tsunami risk for the Mediterranean and connected seas can be obtained using complete data sets than incomplete and uncertain historical impact records. Specifically for the Black Sea, the authors found that the tsunami risk is lowest compared to the other parts of the studied area, examining 22 tsunami events—10 historical (fifth century BC to 1899 AD) and 12 for the instrumental period (1900–2021). It should be noted that for the instrumental period of registered seis-

mic events from the beginning of the last century, there are a small number of registered tsunami events by tide gauge observations along the Black Sea coast, especially for the western part. Also, a comprehensive tsunami hazard and risk analysis are difficult due to the incompleteness and uncertainties of all data files. Therefore, as an initial step to clarify the tsunamigenic potential of the seismic zones in the Black Sea region, the parameters of the active or potentially active faults that can generate earthquakes with a magnitude greater than $M > 5.0$ should be clarified. So far, geophysical and seismic studies, apart from some exceptions, are rare in this region. The exchange of seismic data between coastal countries is one of the obstacles to a comprehensive and in-depth analysis of the seismic activity in the region as a whole. Furthermore, the ambiguous attachment of specific focal mechanisms of earthquakes to active faults or their segments leads to contradictory results, complicating the subsequent analysis and interpretation of seismic and tsunami hazards and risks. Therefore, conducting detailed interdisciplinary research for local or site-specific assessments is necessary, including collecting data and evidence from past tsunami events.

We compiled the BSE catalog based on statistical data processing and calculation procedures with the specialized software ZMAP [65], analyzing many seismic events realized at different seismic sources and registered by different sensors. Therefore, the results of our research have certain limitations of a different nature. For example, some of them are due to the completeness, accuracy, and reliability of the data sets contained in the analyzed catalogs. Regarding data completeness, it should be noted that the analyzed data may not include all seismic events, especially those that were of low magnitude or unreported, due to different procedures used by seismic data centers. Also, data on seismic events can be subject to various sources of error, such as sensor issues or data transmission disruptions. Due to the absence or poorly presented seismic data in all analyzed datasets, there are certain incompletenesses in the compiled BSE catalog, which is evident for the Northern and Eastern Polygons in the studied region. In complex cases or ambiguous seismic events, subjective decisions may affect the inaccurate representation of seismic events in the studied region. Also, we derived linear dependences for transformation from different magnitude scales into moment magnitude M_w for the corresponding geographic polygon using different numbers of events. The number of seismic event pairs available to derive these linear relationships is critical in estimating the parameters of the corresponding linear regression. Other factors that should be considered are the calculation procedures and software algorithms, where expert knowledge is used in analyzing and interpreting the results, for example, in the procedure for declustering, applying the Reasenber algorithm [62].

Further work is needed (1) to include seismic events, which are not so far included in the BSE catalog, to complement and improve it; (2) for detailed local studies to identify potentially active faults triggering earthquakes with tsunamigenic potential; (3) to derive unambiguous empirical dependences when transforming between different magnitude scales into moment magnitude for the identified seismically active seismic zones, and (4) to derive maximum-likelihood parameters used as inputs in modeling and simulations of earthquake-triggered tsunamis in the study area.

7. Conclusions

We used freely available data catalogs of four international data centers, namely USGS, ISC, EMSC, and five national catalogs, respectively, Romanian, Turkish, Bulgarian, and published catalog information on events on the territory of Russia to compile a new catalog of the Black Sea earthquakes. Initially, the summary catalog of earthquakes from 1905 to 2022 in the specified region $27^\circ \text{ E} - 42^\circ \text{ E}$ and $40^\circ \text{ N} - 47^\circ \text{ N}$ included 54,918 earthquakes. First, we calculated numerically empirical model dependencies for five geographically defined polygons to convert magnitudes from heterogeneous locally reported magnitude scales into standard proxy magnitude scales equivalent to the moment magnitude M_w . Second, a declustering procedure was applied to remove duplicate events. As a result, a catalog of precisely defined earthquakes in the Black Sea region was compiled, comprising 54,647 events, and published in CSV format under an open license. The created catalog can

be helpful to seismologists, geologists, and other specialists studying seismic phenomena in the Black Sea region. The BSE catalog will be freely available and can be regularly updated, including recent earthquakes registered by the available and updated national seismic networks in the studied region. In addition, the part of the homogenized catalog from 1977 to 2022 related to the instrumental monitoring of the seismicity of the Black Sea region is studied. A declustering procedure was applied to remove duplicate events in the catalog. The catalog comprises as many as 18,528 unique earthquakes within the magnitude range from 2.5 to 6.1 ($2.5 \leq M_w \leq 6.1$) and realized at a depth not more than 40 km. Then, the quality of the newly compiled catalog was assessed by evaluating the magnitude of completeness M_c and its uncertainty. According to the Gutenberg–Richter law, the frequency–magnitude distribution is calculated. The magnitude of completeness is equal to 2.5 ($M_c = 2.5$), and the b -value and the a -value are 1.17 (± 0.01) and 7.192, respectively. Based on the three parameters' estimations, we can conclude that the new BSE catalog is representative and can be used in the presented study and for further seismic and tsunami hazard analyses of the Black Sea region.

The spatial distribution of the magnitude of completeness shows as follows: the Northwestern, Western, and Southern Polygons demonstrate the lowest values of M_c below 3; the regions of Southern Crimea and Western Russia (parts of the NP and the EP) have completeness magnitudes around 3.5, for which, the most likely reason is a lack of free available catalogs. The spatial distribution of the b -value is obtained and plotted on the map, delineating areas of low values in the WP and the EP, and areas of relatively higher values in the SP and the NWP. Making a separate spatio-temporal analysis for specific low-lying locations along the Black Sea coast is necessary to obtain more meaningful results in studying the tsunamigenic potential of seismically active fault zones. Finally, the strongest earthquakes with a magnitude above 5 ($M_w \geq 5$), which are realized in the studied region, are estimated based on their focal mechanisms and spatial–temporal distribution.

In this study, newly collected and analyzed information about the seismic regime during the last century in the Black Sea region shows that the probability of a strong earthquake in the future should not be underestimated. Tsunamis in the Black Sea are not as large, destructive, and frequent as in other tsunami-prone areas. However, the tsunami risk for some local Black Sea coastal areas such as the Balchik–Kaliakra region (Northeastern Bulgaria), Northwestern Turkey, the southern coast of the Crimean Peninsula, and the western coast of Georgia is relatively high compared to others and should be studied in detail.

Author Contributions: Conceptualization, E.O., L.D., and L.P.; methodology, E.O. and L.D.; software, E.O.; investigation, E.O., L.D., and L.P.; formal analysis, E.O., L.D., L.P., and D.D.; data curation, E.O., L.D., and D.D.; writing—original draft preparation, E.O., L.D., and L.P.; writing—review and editing, E.O., L.D., L.P., and D.D.; visualization, E.O. and L.P.; project administration, L.P.; funding acquisition, L.P. All authors have read and agreed to the published version of the manuscript.

Funding: This study was funded by the Bulgarian National Science Fund under the Contract KII-06-KOCT/8. It contributes to the European Cooperation in Science and Technology COST project “AGITHAR—Accelerating Global Science in Tsunami Hazard and Risk Analysis”.

Data Availability Statement: The newly compiled regional seismic catalog for the Black Sea region (BSEC) will be published at <https://zenodo.org/badge/DOI/10.5281/zenodo.8070409.svg> (accessed on 22 June 2023). All data used for this study were mentioned in the text and relevant data sources are properly cited. Data analysis was performed using ZMAP and Matlab tools. Figure 1 was created through Global Mapper[®], and the rest of the figures were created by ZMAP and Matlab.

Acknowledgments: The authors are grateful to the World Data Centres USGS, ISC, EMSC, and IDC for the freely available seismic data catalogs, as well as to the seismologists on duty at the National Operative Telemetric System for Seismological Information (NOTSSI) operated by the National Institute of Geophysics, Geodesy, and Geography at the Bulgarian Academy of Sciences. We acknowledge Dogan Kalafat and Didem Musavver for providing data from the Turkish seismic catalog.

Conflicts of Interest: The authors declare no conflict of interest. The funders had no role in the study's design; in the collection, analyses, or interpretation of data; in the writing of the manuscript; or in the decision to publish the results. The authors are not responsible for any consequences arising from the reuse of this publication.

References

1. Behrens, J.; Løvholt, F.; Jalayer, F.; Lorito, S.; Salgado-Gálvez, M.A.; Sørensen, M.; Abadie, S.; Aguirre-Ayerbe, I.; Aniel-Quiroga, I.; Babeyko, A.; et al. Probabilistic Tsunami Hazard and Risk Analysis: A Review of Research Gaps. *Front. Earth Sci.* **2021**, *9*, 628772. [[CrossRef](#)]
2. Cugliari, L.; Cerase, A.; Amato, A. Tsunami risk perception, a state-of-the-art review with a focus in the NEAM region. *Front. Earth Sci.* **2022**, *10*, 995536. [[CrossRef](#)]
3. Reid, J.A.; Mooney, W.D. Tsunami Occurrence 1900–2020: A Global Review, with Examples from Indonesia. *Pure Appl. Geophys.* **2022**, *180*, 1549–1571. [[CrossRef](#)]
4. Hu, G.; Feng, W.; Wang, Y.; Li, L.; He, X.; Karakaş, Ç.; Tian, Y. Source Characteristics and Exacerbated Tsunami Hazard of the 2020 Mw 6.9 Samos Earthquake in Eastern Aegean Sea. *J. Geophys. Res. Solid Earth* **2022**, *127*, e2022JB023961. [[CrossRef](#)]
5. Geist, E.L.; Parsons, T. Probabilistic Analysis of Tsunami Hazards. *Nat. Hazards* **2006**, *37*, 277–314. [[CrossRef](#)]
6. Løvholt, F.; Griffin, J.; Salgado-Gálvez, M. Tsunami Hazard and Risk Assessment on the Global Scale. In *Encyclopedia of Complexity and Systems Science*; Meyers, R., Ed.; Springer: Berlin/Heidelberg, Germany, 2015. [[CrossRef](#)]
7. Selva, J.; Amato, A.; Armigliato, A.; Basili, R.; Bernardi, F.; Brizuela, B.; Cerminara, M.; Vitturi, M.D.M.; Di Bucci, D.; Di Manna, P.; et al. Tsunami risk management for crustal earthquakes and non-seismic sources in Italy. *Riv. Nuovo Cim.* **2021**, *44*, 69–144. [[CrossRef](#)]
8. Papadopoulos, G.A.; Imamura, F.; Nosov, M.; Charalampakis, M. Tsunami magnitude scales. In *Geological Records of Tsunamis and Other Extreme Waves*, 1st ed.; Engel, M., Pilarczyk, J., May, S.M., Brill, D., Garrett, E., Eds.; Elsevier: Amsterdam, The Netherlands, 2020; pp. 33–46. [[CrossRef](#)]
9. Papadopoulos, G.A.; Diakogianni, G.; Fokaefs, A.; Ranguelov, B. Tsunami hazard in the Black Sea and the Azov Sea: A new tsunami catalogue. *Nat. Hazards Earth Syst. Sci.* **2011**, *11*, 945–963. [[CrossRef](#)]
10. Papadopoulos, G.A.; Gràcia, E.; Urgeles, R.; Sallares, V.; De Martini, P.M.; Pantosti, D.; González, M.; Yalçiner, A.C.; Mascle, J.; Sakellariou, D.; et al. Historical and pre-historical tsunamis in the Mediterranean and its connected seas: Geological signatures, generation mechanisms and coastal impacts. *Mar. Geol.* **2014**, *354*, 81–109. [[CrossRef](#)]
11. Dimova, L.; Armigliato, A.; Pagnoni, G.; Tinti, S.; Raykova, R. Atmosphere and Space Tsunami Radiation Pattern from Seismic Sources in the Black Sea. In Proceedings of the 3rd National Congress on Physical Sciences, Section: Physics of Earth, Sofia, Bulgaria, 29 September–2 October 2016; Available online: <http://upb.phys.uni-sofia.bg/conference/3kongres/disk/html/pdf/S0655.pdf> (accessed on 7 June 2023).
12. Nikonov, A.; Gusiakov, V.; Fleifel', L. Assessment of the tsunami hazard on the Russian coast based on a new catalogue of tsunamis in the Black Sea and the Sea of Azov. *Russ. Geol. Geophys.* **2018**, *59*, 193–205. [[CrossRef](#)]
13. Cambaz, M.D.; Turhan, F.; Yılmaz, M.; Kekovalı, K.; Necmioğlu, Ö.; Kalafat, D. An Investigation on the Evaluation of Seismic Network and Catalogue of Regional Earthquake-Tsunami Monitoring Center (RETMK-KOERI). *Yerbilimleri* **2019**, *40*, 110–135. [[CrossRef](#)]
14. Grigorash, Z.K. Review of remote tide gauge records of some tsunamis in the Black Sea. In *Trudy SakhKNII, SahKNII*; Far East Scientific Center, USSR Academy of Sciences: Sakhalin, Russia, 1972; pp. 271–278.
15. Dotsenko, S.F.; Konovalov, A.V. Tsunami waves in the Black Sea in 1927: Observations and numerical modelling. *Phys. Oceanogr.* **1996**, *7*, 389–401. [[CrossRef](#)]
16. Pelinovsky, E. Preliminary estimates of tsunami danger for the northern part of the Black Sea. *Phys. Chem. Earth Part A* **1999**, *24*, 175–178. [[CrossRef](#)]
17. Dotsenko, S.F.; Ingerov, A.V. Characteristics of tsunami waves in the Black Sea according to the data of measurements. *Phys. Oceanogr.* **2007**, *17*, 17–28. [[CrossRef](#)]
18. Yalçiner, A.; Pelinovsky, E.; Talipova, T.; Kurkin, A.; Kozelkov, A.; Zaitsev, A. Tsunamis in the Black Sea: Comparison of the historical, instrumental, and numerical data. *J. Geophys. Res. Atmos.* **2004**, *109*, C12023. [[CrossRef](#)]
19. Altınok, Y.; Alpar, B.; Özer, N.; Aykurt, H. Revision of the tsunami catalogue affecting Turkish coasts and surrounding regions. *Nat. Hazards Earth Syst. Sci.* **2011**, *11*, 273–291. [[CrossRef](#)]
20. Mazova, R.; Kiselman, B.; Kolchina, E. Numerical simulation of tsunami wave height distribution for Turkish Black Sea coast in nonlinear dynamic keyboard model of underwater seismic source. *J. Comput. Appl. Math.* **2014**, *259*, 887–896. [[CrossRef](#)]
21. Partheniu, R.; Diaconescu, M.; Ioane, D.; Marmureanu, A. Tsunami Modeling Scenarios for Some of the Seismic Sources in the Black Sea Area, Using Tsunami Analysis Tool Software. In Proceedings of the 8th Congress of the Balkan Geophysical Society, Chania, Greece, 5–8 October 2015; pp. 1–5. [[CrossRef](#)]
22. Moldovan, I.A.; Diaconescu, M.; Partheniu, R.; Constantin, A.P.; Popescu, E.; Toma-Danila, D. Probabilistic seismic hazard assessment in the Black Sea area. *Rom. J. Phys.* **2017**, *62*, 809.
23. Bazykina, A.Y.; Mikhailichenko, S.Y.; Fomin, V.V. Numerical Simulation of Tsunami in the Black Sea Caused by the Earthquake on September 12, 1927. *Phys. Oceanogr.* **2018**, *25*, 295–304. [[CrossRef](#)]

24. Dimova, L.; Raykova, R. Tsunami Hazard on the Black Sea Coast by Numerical Modelling. *C. R. Acad. Bulg. Sci.* **2018**, *71*, 350–1356. [[CrossRef](#)]
25. Baranova, E.A.; Mazova, R.K. Tsunami Hazard for the Crimean Coast of the Black Sea and the Kerch Strait at the Catastrophic Tsunamigenic Earthquakes, the Locations of which are Close to that of the Historical Yalta Earthquake on 12 September 1927. *Phys. Oceanogr.* **2020**, *27*, 110–125. [[CrossRef](#)]
26. Emre, Ö.; Duman, T.Y.; Özalp, S.; Şaroğlu, F.; Olgun, Ş.; Elmacı, H.; Çan, T. Active fault database of Turkey. *Bull. Earthq. Eng.* **2016**, *16*, 3229–3275. [[CrossRef](#)]
27. Gobarenko, V.S.; Murovskaya, A.V.; Yegorova, T.P.; Sheremet, E.E. Collision processes at the northern margin of the Black Sea. *Geotectonics* **2016**, *50*, 407–424. [[CrossRef](#)]
28. Shumlyanskaya, L.A.; Burmin, V.Y. Parameters of the fault planes for the Crimean Black Sea region by averaged mechanism of close earthquakes. *Geofiz. Zhurnal.* **2017**, *38*, 100–116. [[CrossRef](#)]
29. Diaconescu, M.; Craiu, A.; Toma–Danila, D.; Craiu, G.M. Main active faults from the eastern part of Romania (Dobrogea and Black Sea). Part I: Longitudinal faults system. *Rom. Rep Phys.* **2019**, *71*, 702.
30. Işcan, Y.; Ocakoğlu, N.; Kılıç, F.; Özel, O. Active tectonics of offshore Cide–Sinop (southern Black Sea shelf): From seismic and multibeam bathymetry data. *Geo-Marine Lett.* **2019**, *39*, 279–294. [[CrossRef](#)]
31. Simmons, M.D.; Tari, G.C.; Okay, A.I. Petroleum geology of the Black Sea: Introduction. *Geol. Soc. London Spec. Publ.* **2018**, *464*, 1–18. [[CrossRef](#)]
32. Triantafyllou, I.; Papadopoulos, G.A.; Kijko, A. Probabilistic Tsunami Risk Assessment from Incomplete and Uncertain Historical Impact Records: Mediterranean and Connected Seas. *Pure Appl. Geophys.* **2023**, *180*, 1785–1809. [[CrossRef](#)]
33. Basili, R.; Tiberti, M.M.; Kastelic, V.; Romano, F.; Piatanesi, A.; Selva, J.; Lorito, S. Integrating geologic fault data into tsunami hazard studies. *Nat. Hazards Earth Syst. Sci.* **2013**, *13*, 1025–1050. [[CrossRef](#)]
34. Zelenin, E.; Bachmanov, D.; Garipova, S.; Trifonov, V.; Kozhurin, A. The Database of the Active Faults of Eurasia (AFEAD): Ontology and Design behind the Continental-Scale Dataset. *Earth Syst. Sci. Data* **2022**, *14*, 4489–4503. [[CrossRef](#)]
35. Dimitrova, L.; Oynakov, E.; Pashova, L.; Dragomirov, D. Assessment of the historical and recent seismicity of the Black Sea region. SGEM2021 Book: 21st International Multidisciplinary Scientific Geo Conference. *Sect. Appl. Environ. Geophys.* **2021**, *21*, 419–426. Available online: <https://www.sgem.org/index.php/jresearch-article?citekey=20215645652> (accessed on 3 June 2023).
36. Solakov, D.; Simeonova, S.; Raikova, P.; Aleksandrova, I. *Catalog of the Earthquakes in Bulgaria and Surroundings since 1981*; Funds NIGGG-BAS; National Institute of Geophysics, Geodesy and Geography-AS: Sofia, Bulgaria, 2020. [[CrossRef](#)]
37. Rangelov, B.; Gospodinov, D. Tsunami vulnerability modelling for the bulgarian black sea coast. *Water Sci. Technol.* **1996**, *32*, 47–53. [[CrossRef](#)]
38. Grünthal, G.; Wahlström, R. The European-Mediterranean Earthquake Catalogue (EMEC) for the last millennium. *J. Seism.* **2012**, *16*, 535–570. [[CrossRef](#)]
39. Storchak, D.A.; Harris, J.; Brown, L.; Lieser, K.; Shumba, B.; Verney, R.; Di Giacomo, D.; Korger, E.I.M. Rebuild of the Bulletin of the International Seismological Centre (ISC), part 1: 1964–1979. *Geosci. Lett.* **2017**, *4*, 32. [[CrossRef](#)]
40. Storchak, D.A.; Harris, J.; Brown, L.; Lieser, K.; Shumba, B.; Di Giacomo, D. Rebuild of the Bulletin of the International Seismological Centre (ISC)—Part 2: 1980–2010. *Geosci. Lett.* **2020**, *7*, 18. [[CrossRef](#)]
41. Dziewonski, A.M.; Chou, T.-A.; Woodhouse, J.H. Determination of earthquake source parameters from waveform data for studies of global and regional seismicity. *J. Geophys. Res. Atmos.* **1981**, *86*, 2825–2852. [[CrossRef](#)]
42. Ekström, G.; Nettles, M.; Dziewoński, A. The global CMT project 2004–2010: Centroid-moment tensors for 13,017 earthquakes. *Phys. Earth Planet. Inter.* **2012**, *200–201*, 1–9. [[CrossRef](#)]
43. Onescu, M.C.; Marza, V.I.; Rizescu, M.; Popa, M. The Romanian earthquake catalog between 984–1997. In *Vrancea Earthquakes: Tectonics, Hazard and Risk Mitigation*; Advances in Natural and Technological Hazards Research; Wenzel, F., Lungu, D., Novak, O., Eds.; Springer: Dordrecht, The Netherlands, 1999; Volume 11, pp. 43–47. [[CrossRef](#)]
44. Kozinenko, N.M.; Svidlova, V.A.; Sykchina, Z.N.; Antonyuk, G.P.; Antonyuk, V.A.; Bondar, M.N.; Kuryanova, I.V.; Lukyanova, Z.N.; Podvintsev, A.V.; Roslyakov, A.V. Catalog and Detailed Data on Earthquakes in the Crimean-Black Sea Region for 2012, Seismological Bulletin of Ukraine for 2012, Sevastopol, SPC “ECOSY-Hydrophysics”. 2013; pp. 57–85. Available online: <http://dspace.nbu.gov.ua/handle/123456789/145810> (accessed on 2 June 2023). (In Russian)
45. Pustovitenko, B.G.; Kalinyuk, I.V.; Merzhej, E.A.; Porechnova, E.I.; Sykchin, Z.N. Dynamic parameters of earthquake foci of the Crimean, Zemletryaseniia Severnoj Evrazii, (Earthquakes of Northern Eurasia). *Geophys. J.* **2008**, *35*, 289–296.
46. Pustovitenko, B.G.; Kalinyuk, I.V.; Merzhej, E.A. Dynamic parameters of earthquake foci of the Crimean—Black Sea region. In *Zemletryaseniia Severnoj Evrazii*; Earthquakes in Northern Eurasia 2010; GS RAS: Obninsk, Russia, 2016; pp. 296–304. Available online: http://www.gsras.ru/zse/uploads/files/eq_ne_2010/2010-Spectra_and_dinamic_param-Dynamic_parameters_Crimean-296-304.pdf (accessed on 1 June 2023). (In Russian)
47. Pustovitenko, B.G.; Kalinyuk, I.V. Earthquake Focus Parameters in the Crimean-Black Sea Region, Zemletryaseniia Severnoj Evrazii, (Earthquakes in Northern Eurasia, 2019). 2013. Volume 22. pp. 296–304. Available online: <https://cyberleninka.ru/article/n/ochagovye-parametry-zemletryasenyi-krymsko-chernomorskogo-regiona> (accessed on 21 June 2023).
48. Pustovitenko, B.G.; Merger, E.A.; Pustovitenko, A.A. Dynamic parameters of the earthquake foci of Crimea according to digital seismic stations. *Geofiz. Zhurnal.* **2013**, *35*, 172–186. [[CrossRef](#)]

49. Pustovitenko, B.G. Updated focal parameters of 1990 earthquakes in Crimea, Scientific notes of the Crimean Federal University named after V. I. Vernadsky. *Geography* **2014**, *27*, 169–178.
50. Pustovitenko, B.G.; Eredzhepov, E.E. Focal parameters of earthquakes in the Crimean-of the Black Sea region 2016, Scientific notes of the V. I. Vernadsky Crimean Federal University. *Geogr. Geol.* **2017**, *3*, 51–69.
51. Pustovitenko, B.G.; Eredzhepov, E.E.; Bondar, M.N. Spectral and dynamic parameters of the foci of 2019 Crimean earthquakes, Scientific notes of the V. I. Vernadsky Crimean Federal University. *Geogr. Geol.* **2020**, *6*, 67–85.
52. Pustovitenko, B.G.; Eredzhepov, E.E. Corrected focal parameters of the earthquakes of the Crimea 2018–2019, Scientific notes of the Crimean Federal University named after V. I. Vernadsky. *Geogr. Geol.* **2021**, *7*, 164–175.
53. Pustovitenko, B.G.; Eredzhepov, E.E. Spectral and dynamic parameters of the foci of 2015 Crimean earthquakes, Scientific notes of the V. I. Vernadsky Crimean Federal University. *Geogr. Geol.* **2021**, *2*, 53–68.
54. Pustovitenko, B.G.; Eredzhepov, E.E.; Bondar, M.N. Spectral and dynamic parameters of the foci of 2020 Crimean earthquakes, Scientific notes of the V. I. Vernadsky Crimean Federal University. *Geogr. Geol.* **2021**, *7*, 70–86.
55. Stromeyer, D.; Grünthal, G.; Wahlström, R. Chi-square regression for seismic strength parameter relations, and their uncertainties, with applications to an M_w based earthquake catalog for central, northern and northwestern Europe. *J. Seismol.* **2004**, *8*, 143–153. [[CrossRef](#)]
56. Das, R.; Wason, H.; Sharma, M. Magnitude conversion to unified moment magnitude using orthogonal regression relation. *J. Asian Earth Sci.* **2012**, *50*, 44–51. [[CrossRef](#)]
57. Castellaro, S.; Mulargia, F.; Kagan, Y.Y. Regression problems for magnitudes. *Geophys. J. Int.* **2006**, *165*, 913–930. [[CrossRef](#)]
58. Scordilis, E.M. Empirical Global Relations Converting M_S and m_b to Moment Magnitude. *J. Seism.* **2006**, *10*, 225–236. [[CrossRef](#)]
59. Gasperini, P.; Lolli, B.; Castellaro, S. Comparative Analysis of Regression Methods Used for Seismic Magnitude Conversions. *Bull. Seism. Soc. Am.* **2015**, *105*, 1787–1791. [[CrossRef](#)]
60. Gilat, A. (Ed.) *MATLAB: An Introduction with Applications*, 5th ed.; John Wiley & Sons: New York, NY, USA, 2014.
61. Celmins, A. The method of Gauss in 1799. *Stat. Sci.* **1998**, *3*, 123–135.
62. Reasenber, P. Second-order moment of central California seismicity, 1969–1982. *J. Geophys. Res. Atmos.* **1985**, *90*, 5479–5495. [[CrossRef](#)]
63. Gardner, J.K.; Knopoff, L. Is the sequence of earthquakes in Southern California, with aftershocks removed, Poissonian? *Bull. Seism. Soc. Am.* **1974**, *64*, 1363–1367. [[CrossRef](#)]
64. Tan, O. A homogeneous earthquake catalogue for Turkey. *Nat. Hazards Earth Syst. Sci.* **2021**, *21*, 2059–2073. [[CrossRef](#)]
65. Wiemer, S. A Software Package to Analyze Seismicity: ZMAP. *Seism. Res. Lett.* **2001**, *72*, 373–382. [[CrossRef](#)]
66. Mignan, A.; Woessner, J. Estimating the magnitude of completeness in earthquake catalogs. *Community Online Resour. Stat. Seism. Anal.* **2012**, 1–45. [[CrossRef](#)]
67. Solakov, D.; Simeonova, S.; Raykova, P.; Aleksandrova, I. Empirical Relations Converting M_d and M_p Magnitudes Applied in Bulgarian Seismological Routine Practice to Moment Magnitude. *C. R. Acad. Bulg. Sci.* **2018**, *71*, 1076–1085. [[CrossRef](#)]
68. Bilim, F.; Aydemir, A.; Ateş, A.; Dolmaz, M.N.; Koşaroğlu, S.; Erbek, E. Crustal thickness in the Black Sea and surrounding region, estimated from the gravity data. *Mar. Pet. Geol.* **2020**, *123*, 104735. [[CrossRef](#)]
69. Wiemer, S. Minimum Magnitude of Completeness in Earthquake Catalogs: Examples from Alaska, the Western United States, and Japan. *Bull. Seism. Soc. Am.* **2000**, *90*, 859–869. [[CrossRef](#)]
70. Woessner, J. Assessing the Quality of Earthquake Catalogues: Estimating the Magnitude of Completeness and Its Uncertainty. *Bull. Seism. Soc. Am.* **2005**, *95*, 684–698. [[CrossRef](#)]
71. Wiemer, S.; Wyss, M. Mapping spatial variability of the frequency-magnitude distribution of earthquakes. *Adv. Geophys.* **2002**, *45*, 259–302. [[CrossRef](#)]
72. Godano, C.; Petrillo, G. Estimating the Completeness Magnitude m_c and the b -Values in a Snap. *Earth Space Sci.* **2023**, *10*, e2022EA002540. [[CrossRef](#)]
73. Amorāse, D.; Grasso, J.-R.; Rydelek, P.A. On varying b -values with depth: Results from computer-intensive tests for Southern California. *Geophys. J. Int.* **2010**, *180*, 347–360. [[CrossRef](#)]
74. Aki, K. Maximum likelihood estimate of b in the formula $\log(N) = a - bM$ and its confidence limits. *Bull. Earthq. Res. Inst. Tokio Univ.* **1965**, *43*, 237–239.
75. Kagan, Y.Y. Universality of the Seismic Moment-frequency Relation. *Pure Appl. Geophys.* **1999**, *155*, 537–573. [[CrossRef](#)]
76. Kagan, Y.Y. Seismic moment distribution revisited: I. Statistical results. *Geophys. J. Int.* **2002**, *148*, 520–541. [[CrossRef](#)]
77. Kagan, Y.Y. Earthquake size distribution: Power-law with exponent $\beta \equiv 12$? *Tectonophysics* **2010**, *490*, 103–114. [[CrossRef](#)]
78. Kamer, Y. Minimum Sample Size for Detection of Gutenberg-Richter's b -Value. 2013. Available online: <https://arxiv.org/ftp/arxiv/papers/1410/1410.1815.pdf> (accessed on 2 June 2023).
79. Kamer, Y.; Hiemer, S. Comment on “Analysis of the b -values before and after the 23 October 2011 Mw 7.2 Van–Erciş, Turkey, earthquake”. *Tectonophysics* **2013**, *608*, 1448–1451. [[CrossRef](#)]
80. Shi, Y.; Bolt, B.A. The standard error of the magnitude-frequency b value. *Bull. Seism. Soc. Am.* **1982**, *72*, 1677–1687. [[CrossRef](#)]
81. Schorlemmer, D.; Wiemer, S.; Wyss, M. Variations in earthquake-size distribution across different stress regimes. *Nature* **2005**, *437*, 539–542. [[CrossRef](#)]
82. Geffers, G.-M.; Main, I.G.; Naylor, M. Biases in estimating b -values from small earthquake catalogs: How high are high b -values? *Geophys. J. Int.* **2022**, *229*, 1840–1855. [[CrossRef](#)]

83. Nasir, A.; Hintersberger, E.; Decker, K. The temporal evolution of seismicity and variability of b-values along the Vienna Basin Transfer Fault System. *Austrian J. Earth Sci.* **2023**, *116*, 1–15. [[CrossRef](#)]
84. Nanjo, K.Z.; Yoshida, A. Changes in the b value in and around the focal areas of the M6.9 and M6.8 earthquakes off the coast of Miyagi prefecture, Japan, in 2021. *Earth, Planets Space* **2021**, *73*, 176. [[CrossRef](#)]
85. Schorlemmer, D.; Wiemer, S.; Wyss, M. Earthquake statistics at Parkfield: 1. Stationarity of b values. *J. Geophys. Res. Atmos.* **2004**, *109*, B12307–B12317. [[CrossRef](#)]
86. Tari, E.; Sahin, M.; Barka, A.; Reilinger, R.; King, R.W.; McClusky, S.; Prilepin, M. Active tectonics of the Black Sea with GPS. *Earth, Planets Space* **2000**, *52*, 747–751. [[CrossRef](#)]
87. Kalafat, D. An Overview of the Seismicity and Tectonics of the Black Sea. In *Moment Tensor Solutions*; D'Amico, S., Ed.; Springer Natural Hazards: Berlin/Heidelberg, Germany, 2018; pp. 573–588. [[CrossRef](#)]
88. Kalafat, D.; Kekovalı, K.; Güneş, Y.; Yilmazer, M.; Kara, M.; Deniz, P.; Berberoglu, M. *A Catalogue of Source Parameters of Moderate and Strong Earthquakes for Turkey and its Surrounding Area (1938–2008)*; Kandili Observatory, Istanbul, Report; Boğaziçi Üniversitesi: Istanbul, Turkey, 2009; 43p. (In Turkish)
89. Oynakov, E.; Dimitrova, L.; Pashova, L.; Dragomirov, D. Analysis of potential seismic sources of tsunamis in the Black Sea region, using data from various catalogs. In Proceedings of the EGU General Assembly 2021, online, 19–30 April 2021. EGU21-8278. [[CrossRef](#)]

Disclaimer/Publisher's Note: The statements, opinions and data contained in all publications are solely those of the individual author(s) and contributor(s) and not of MDPI and/or the editor(s). MDPI and/or the editor(s) disclaim responsibility for any injury to people or property resulting from any ideas, methods, instructions or products referred to in the content.